A MODEL-FOLLOWING NEURO-ADAPTIVE APPROACH FOR ROBUST CONTROL OF HIGH PERFORMANCE AIRCRAFTS

Radhakant Padhi [*], **P. Narayana Rao** [**], **Siddharth Goyal** [***], **Abha Tripathi** [****]

[*] *Asst. Professor, Dept. of Aerospace Eng., Indian Institute of Science (IISc), Bangalore, India.*
[**] *Former Graduate Student, Dept. of Aerospace Eng., IISc, Bangalore, India.*
[***] *Former Summer Trainee, Dept. of Aerospace Eng., IISc, Bangalore, India.*
[****] *Former Project Assistant, Dept. of Aerospace Eng., IISc, Bangalore, India.*

Abstract: Based on dynamic inversion, a relatively straightforward approach is presented in this paper for nonlinear flight control design of high performance aircrafts, which does not require the normal and lateral acceleration commands to be first transferred to body rates before computing the required control inputs. This leads to substantial improvement of the tracking response. Promising results are obtained from six degree-of-freedom simulation studies of F-16 aircraft, which are found to be superior as compared to an existing approach (which is also based on dynamic inversion). The new approach has two potential benefits, namely reduced oscillatory response (including elimination of non-minimum phase behavior) and reduced control magnitude. Next, a model-following neuron-adaptive design is augmented the nominal design in order to assure robust performance in the presence of parameter inaccuracies in the model. Note that in the approach the model update takes place adaptively online and hence it is philosophically similar to indirect adaptive control. However, unlike a typical indirect adaptive control approach, there is no need to update the individual parameters explicitly. Instead the inaccuracy in the system output dynamics is captured directly and then used in modifying the control. This leads to faster adaptation, which helps in stabilizing the unstable plant quicker. The robustness study from a large number of simulations shows that the adaptive design has good amount of robustness with respect to the expected parameter inaccuracies in the model.

Keywords: Dynamic inversion, neuro-adaptive design, aircraft control, longitudinal maneuver, lateral maneuver, pilot command tracking, autopilot design

1. INTRODUCTION

To enhance the maneuverability and increase the lift-to-drag ratio, high performance aircrafts are often designed to be naturally unstable. Such aircrafts are also often required to operate at the edge of the flight envelope for combat superiority, which is supposed to be as wide as possible. Besides, the flight dynamics of such aircrafts are also inherently highly nonlinear (they are very often forced to fly in high angle of attack regime) and the aerodynamics involved is also quite complex. Because of these reasons, the flight control design for

high-performance aircrafts is a very challenging task. Traditional control system design techniques based on classical control theory are becoming increasingly inadequate to meet the stringent performance requirements with assured stability and there is a strong need to use modern control design methods. Many modern control design techniques have been attempted to come up with effective flight control design, the task of which is essentially to track the pilot commands while simultaneously assuring stability and robustness of the overall plant. Techniques such as H_∞ robust control design [Lin et al., 1997], sliding mode control [Schumacher, Cottrill & Yeh, 1999], model-reference control [Bodson, 2002], adaptive control [Ying et al., 2004], intelligent control designs like neuro-control [Willis, 1999], fuzzy-logic control [Won et al., 1999] etc. have been attempted in the literature.

Gain scheduled control design, where a number of gains are first designed at various expected operating points in the flight envelope which are then interpolated based on some physically meaningful scheduling variable(s) is perhaps a very intuitive basic design approach that has found wide acceptability in industry. This philosophy has also been used for control design of high performance aircraft [Lee & Spillman, 1997, Shin, Balas & Kaya, 2001]. However, potential disadvantages of gain scheduling control design include a long tuning process, no theoretical guarantee of stability for the interpolated gain (which is a major concern for unstable plants like unstable aircrafts) etc.

Out of the many advanced techniques that have appeared in the literature, a promising approach is based on the idea of optimal sliding mode [Schumacher, Cottrill & Yeh, 1999], where a two-loop structures has been designed for tracking pilot commands (which are assumed to be angle of attack, roll angle commands while assuring near-zero side slip angle). In this approach, an optimal sliding surface is generated using a state dependent Riccati equation (SDRE) based optimal controller. This is followed by a sliding controller in the inner loop using Lyapunov theory. The performance of this controller has been evaluated using the six degree-of-freedom nonlinear model of F-16 aircraft. Note that SDRE approach can only assure suboptimality and local stability [Cloutier, 1997], and hence such an approach is inadequate for the wide range of flight conditions.

A popular technique, which serves as a 'universal gain scheduling controller' (and hence avoids the tedious gain scheduling process), is dynamic inversion [Enns et al., 1994, Kim & Calise, 1997, Kaneshige, Bull & Totah, 2000, Khalil, 2002]. This technique is essentially based on the technique of feedback linearization. It leads to a number of potential advantages; namely asymptotic (rather exponential) stability of the error dynamics thereby leading to perfect tracking, a simple closed form expression for the controller (hence no computational concerns), preserving many of the benefits of the PID design etc. However, as the dynamic inversion is rather sensitive to the issue of parameter inaccuracy and modeling errors, there is a strong need of augmenting this technique with some other robust/adaptive techniques, to make it useful in practice. A potential approach in this regard is the idea of online dynamic function approximation taking the help of evolving methods like 'neuro-adaptive technique' [Kim & Calise, 1997]. The main philosophy that is exploited heavily in system theory applications is that neural networks have the universal function approximation property, which helps a controller to adapt to plants having unmodelled dynamics and time-varying parameters.

First, assuming perfect knowledge about the plant, this paper proposes a new relatively straightforward approach based on dynamic inversion which is applied for flight control design and the results are compared with an existing approach which is also based on dynamic inversion [Menon, 1993]. The innovations of the current approach as compared to the existing approach include (i) elimination of the necessity of transferring the normal and lateral acceleration commands to equivalent body rate commands before computing the control surface defections (which is usually done in practice), (ii) reduction of tuning parameters in the control design process, (iii) the assumption that double derivative of velocity vector components in body X and Y directions to be is zero, which is a more realistic assumption as compared to assuming their single derivatives to be zero and (iv) elimination of the assumption that double derivative of desired Euler angles are zero. Note that the new approach leads to reduction of control magnitude and reduced oscillatory response. It also substantially reduces nonminimum phase behaviour of the closed loop response. The proposed method is applied for longitudinal and lateral control of F-16 aircraft. Combined longitudinal and lateral control (velocity vector roll) has also been experimented in the numerical simulation studies. The pilot commands assumed in longitudinal mode are normal acceleration and forward velocity of the aircraft. In lateral mode, roll rate and the desired velocity are used as pilot commands. In the approach, the fast dynamics corresponding to states i.e. body rates which are controlled by the inputs (i.e. aileron, elevator and rudder deflection) are updated for every time step Δt, while slow dynamics corresponding to state total velocity which is controlled by thrust is updated after every five time steps. Promising results are obtained from the fully six-degree-of-freedom (6-DOF) nonlinear simulation, which are found to be superior as compared to an existing approach [Menon, 1993].

Unfortunately, even though the dynamic inversion technique has evolved as a promising tool for nonlinear control design substituting the extensive gain scheduling approach, there are a few important issues with respect to the technique as well. Because of modeling error and parameter inaccuracies, inver-

sion of the model does not lead to exact cancelation of the nonlinearities. Because of this, the technique becomes sensitive to the parameter inaccuracies and unmodelled dynamics, and hence, there is a need to augment this technique with adaptive/robust control design tools. This problem of sensitivity to parameter inaccuracies (both aerodynamic and inertia parameter inaccuracies) is addressed next by augmenting the dynamic inversion technique with a neuro-adaptive design approach [Padhi, 2007], the basic philosophy of which has been recently proposed by the first author of this paper along with his earlier co-workers. This adaptive control design is carried out in two steps: (i) synthesis of a set of neural networks which capture matched unmodelled (neglected) dynamics or model uncertainties because of parametric variations and (ii) synthesis of a controller that drives the state of the actual plant to that of a desired nominal model. The neural network weight update rule is derived using Lyapunov theory, which guarantees both stability of the error dynamics (in a practical stability sense) and boundedness of the weights of the neural networks. Note that even though this technique has been used along with dynamic inversion technique, the basic philosophy and procedure is independent of the technique used to design the nominal controller, and hence can be used in conjunction with any known control design technique. An interested reader can see the reference for details of this approach. However, for completeness of this paper, the necessary steps are given in a subsequent section of this paper (including all design parameters). Note that the proposed approach in this paper is slightly different from the one proposed in [Padhi, 2007]. This is because here we are particularly interested in the output robustness (i.e. performance robustness), where as in the reference cited the primary focus was to enhance stability (i.e. robust stability). In the aircraft problem discussed in this paper, a robustness study from large number of simulations has been carried out by randomly varying the parameters (this has been done due to lack of precise mathematical tools for rigorous mathematical analysis). This study clearly shows that the control design has good amount of robustness with respect to expected levels of parameter inaccuracies in the model. Note that in the approach the model update takes place adaptively online and hence it is philosophically similar to indirect adaptive control. However, unlike a typical indirect adaptive control approach, there is no need to update the individual parameters explicitly. Instead the inaccuracy in the system output dynamics is captured directly and then used in modifying the control. This leads to faster adaptation, which helps in stabilizing the unstable plant quicker.

2. NONLINEAR SIX-DOF AIRCRAFT DYNAMICS

2.1 Equations of motion

Assuming the airplane to be a rigid body and earth to be flat, the complete set of Six-DOF equations of motion in the body frame are given by the following set of differential equations [Roskam, 1995].

$$\dot{U} = RV - QW - g\sin\Theta + (F_{A_x} + T)/m \tag{1}$$

$$\dot{V} = PW - RU + g\cos\Theta\sin\Phi + F_{A_y}/m \tag{2}$$

$$\dot{W} = QU - PV + g\cos\Theta\cos\Phi + F_{A_z}/m \tag{3}$$

$$\dot{P} = c_1QR + c_2PQ + c_3L_A + c_4N_A \tag{4}$$

$$\dot{Q} = c_5PR + c_6(R^2 - P^2) + c_7M_A \tag{5}$$

$$\dot{R} = c_8PQ - c_2QR + c_4L_A + c_9N_A \tag{6}$$

$$\dot{\Phi} = P + Q\sin\Phi\tan\Theta + R\cos\Phi\tan\Theta \tag{7}$$

$$\dot{\Theta} = Q\cos\Phi - R\sin\Phi \tag{8}$$

$$\dot{\Psi} = (Q\sin\Phi + R\cos\Phi)\sec\Theta \tag{9}$$

$$\begin{bmatrix} \dot{x}_E \\ \dot{y}_E \\ \dot{z}_E \end{bmatrix} = \begin{bmatrix} \cos\Psi & -\sin\Psi & 0 \\ \sin\Psi & \cos\Psi & 0 \\ 0 & 0 & 1 \end{bmatrix} \begin{bmatrix} \cos\Theta & 0 & \sin\Theta \\ 0 & 1 & 0 \\ -\sin\Theta & 0 & \cos\Theta \end{bmatrix} \begin{bmatrix} 1 & 0 & 0 \\ 0 & \cos\Phi & -\sin\Phi \\ 0 & \sin\Phi & \cos\Phi \end{bmatrix} \begin{bmatrix} U \\ V \\ W \end{bmatrix} \tag{10}$$

where

$$\begin{bmatrix} c_1 \\ c_2 \\ c_3 \\ c_4 \\ c_8 \\ c_9 \end{bmatrix} \triangleq \frac{1}{(I_{XX}I_{ZZ} - I_{XZ}^2)} \begin{bmatrix} I_{ZZ}(I_{YY} - I_{ZZ}) - I_{XZ}^2 \\ I_{XZ}(I_{ZZ} + I_{XX} - I_{YY}) \\ I_{ZZ} \\ I_{XZ} \\ I_{XZ}^2 + I_{XX}(I_{XX} - I_{YY}) \\ I_{XX} \end{bmatrix}$$

$$\begin{bmatrix} c_5 & c_6 & c_7 \end{bmatrix}^T \triangleq \frac{1}{I_{YY}} \begin{bmatrix} (I_{ZZ} - I_{XX}) & I_{XZ} & 1 \end{bmatrix}^T$$

In the above equations U, V, W are the velocity components and P, Q, R are the roll, pitch and yaw rates respectively about the body-fixed axes. Φ, Θ, Ψ are the Euler angles and x_E, y_E, z_E are the coordinates of ground fixed inertial frame [Roskam, 1995]. Note that $\dot{h} = -\dot{z}_E$ where h is the height of the aircraft from ground. $F_{A_x}, F_{A_y}, F_{A_z}$ are the aerodynamic components of external forces and T is thrust acting along the body X-axis (it is assumed that thrust passes through CG and produces no moment component). Similarly, L_A, M_A, N_A are the aerodynamic components of the airplane. $I_{XX}, I_{YY}, I_{ZZ}, I_{XZ}$ represent the moment of inertias of the airplane in the body frame(note that the aircraft is assumed to be symmetric about the XZ plane and hence, $I_{XY} = I_{XZ} = 0$). m and g represent mass and acceleration due to gravity respectively (both assumed constants).

2.2 Aerodynamic forces and moments

The aerodynamic forces and moments along and about the body X, Y, Z directions are given by [Nguyen et al., 1979].

$$\begin{bmatrix} F_{A_X} & F_{A_Y} & F_{A_Z} \end{bmatrix}^T = \bar{q}S \begin{bmatrix} C_{X_t} & C_{Y_t} & C_{Z_t} \end{bmatrix}^T \quad (11)$$

$$\begin{bmatrix} L_A & M_A & N_A \end{bmatrix}^T = \bar{q}S \begin{bmatrix} bC_{L_t} & \bar{c}C_{M_t} & bC_{N_t} \end{bmatrix}^T \quad (12)$$

where $\bar{q}$ is the dynamic pressure and S is wing platform area. The non-dimensional aerodynamic force coefficients $C_{X_t}, C_{Y_t}, C_{Z_t}$ and the moment coefficients $C_{L_t}, C_{M_t}, C_{N_t}$ are expressed as multivariate nonlinear functions [Morelli, 1998] and are given by

$$C_{X_t} = C_x(\alpha, \delta_e) + C_{x_q}(\alpha)\tilde{q} \quad (13)$$

$$C_{Y_t} = C_y(\beta, \delta_a, \delta_r) + C_{y_p}(\alpha)\tilde{p} + C_{y_r}(\alpha)\tilde{r} \quad (14)$$

$$C_{Z_t} = C_z(\alpha, \beta, \delta_e) + C_{z_q}(\alpha)\tilde{q} \quad (15)$$

$$\begin{aligned} C_{L_t} = {} & C_l(\alpha, \beta) + C_{l_p}(\alpha)\tilde{p} + C_{l_r}(\alpha)\tilde{r} \\ & + C_{l_{\delta_a}}(\alpha, \beta)\delta_a + C_{l_{\delta_r}}(\alpha, \beta)\delta_r \end{aligned} \quad (16)$$

$$C_{M_t} = C_m(\alpha, \delta_e) + C_{m_q}(\alpha)\tilde{q} + C_{Z_t}(x_{cg_{ref}} - x_{cg}) \quad (17)$$

$$\begin{aligned} C_{N_t} = {} & C_n(\alpha, \beta) + C_{n_p}(\alpha)\tilde{p} + C_{n_r}(\alpha)\tilde{r} \\ & + C_{n_{\delta_a}}(\alpha, \beta)\delta_a \\ & + C_{n_{\delta_r}}(\alpha, \beta)\delta_r - C_{Y_t}(x_{cg_{ref}} - x_{cg})(\frac{\bar{c}}{b}) \end{aligned} \quad (18)$$

where $\tilde{p} \triangleq pb/2V$, $\tilde{q} \triangleq q\bar{c}/2V$, $\tilde{r} \triangleq rb/2V$ and $x_{cg_{ref}} \triangleq x_{cg}$.

The following physical data of F-16 used was obtained from [Nguyen et al., 1979]. $m = 637.14$ $slugs$, $S = 300$ ft^2, $b = 30$ ft, $\bar{c} = 11.32\,ft$, $I_{XX} = 9496$ $slugs - ft^2$, $I_{YY} = 55814$ $slugs - ft^2$, $I_{ZZ} = 63100$ $slugs - ft^2$, $I_{XZ} = 982$ $slugs - ft^2$. All of the actuators are modeled as first order lags with limits on deflection and rates [Nguyen et al., 1979]. The thrust actuator has unity gain and rate limit of 10000 lb/sec. The elevator, aileron and rudder each has a gain of (1/0.0495) sec^{-1} and rate limits of ± 60 deg/sec, ± 80 deg/sec, ± 120 deg/sec respectively.

In this paper the velocity vector roll maneuver is also considered. During a velocity vector roll, the aircraft rotates about an axis aligned with its velocity vector. In this case it is convenient to use the wind frame, in which the equation of motion of the aircraft are written as [Wang & Stengel, 2005]

$$\dot{V}_T = (F_{wx}/m) - gsin\gamma \quad (19)$$

$$\dot{\alpha} = Q - (Q_w/cos\beta) - Pcos\alpha tan\beta - Rsin\alpha tan\beta \quad (20)$$

$$\dot{\beta} = R_w + Psin\alpha - Rcos\alpha \quad (21)$$

$$P_w = Pcos\alpha cos\beta + (Q - \dot{\alpha})sin\beta + Rsin\alpha cos\beta \quad (22)$$

$$Q_w = -(F_{wz}/mV_T) - (g/V_T)cos\gamma cos\phi \quad (23)$$

$$R_w = (F_{wy}/mV_T) + (g/V_T)cos\gamma sin\phi \quad (24)$$

$$\dot{\varphi} = P_w + Q_w \sin\varphi \tan\gamma + R_w \cos\varphi \tan\gamma \quad (25)$$

$$\dot{\gamma} = Q_w \cos\varphi - R_w \sin\varphi \quad (26)$$

$$\dot{\psi} = (Q_w \sin\varphi + R_w \cos\varphi)\sec\gamma \quad (27)$$

where V_T, α, β are the total velocity, angle of attack and side slip angle respectively and P_w, Q_w, R_w are the roll, pitch and yaw rates respectively about the wind axes and α is the angle of attack. φ, γ, ψ are the wind-axis Euler angles and F_{wx} is the wind axis total force.

2.3 Equations in compact notation

First, equations (1)-(6) are written in a structured form as follows.

$$\dot{X}_V = f_V(X) + \begin{bmatrix} g_V(X) & d_V \end{bmatrix} \begin{bmatrix} U_A \\ \sigma_T \end{bmatrix} \quad (28)$$

$$\dot{X}_R = f_R(X) + g_R(X)U_A \quad (29)$$

where, $X \triangleq [V_T\ \alpha\ \beta\ P\ Q\ R\ \Phi\ \Theta\ h]^T$, $X_V \triangleq [U\ V\ W]^T$, $X_R \triangleq [P\ Q\ R]^T$, $U_A \triangleq [\delta_a\ \delta_e\ \delta_r]^T$, $\sigma_T \triangleq T/T_{max}$, $U_c \triangleq \begin{bmatrix} U_A^T & \sigma_T \end{bmatrix}^T$.

Note that $\dot{\Psi}$, $\dot{x}_E$, $\dot{y}_E$ are not considered as part of the state equation, as they are not coupled with the other equations (due to the flat earth assumption). Other terms in Equations (28) - (29) are defined as follows.

$$f_{V_1} \triangleq \begin{bmatrix} RV - QW - g\sin\Theta \\ PW - RU + g\cos\Theta\sin\Phi \\ QU - PV + g\cos\Theta\cos\Phi \end{bmatrix}$$

$$f_{V_2} \triangleq \frac{\bar{q}S}{m} \begin{bmatrix} C_x(\alpha) + C_{x_q}(\alpha)\tilde{q} \\ C_y(\beta) + C_{y_p}(\alpha)\tilde{p} + C_{y_r}(\alpha)\tilde{r} \\ C_z(\alpha, \beta) + C_{x_q}(\alpha)\tilde{q} \end{bmatrix}$$

$$g_V(X) \triangleq \frac{\bar{q}S}{m} \begin{bmatrix} 0 & C_{x_{\delta_e}} & 0 \\ C_{y_{\delta_a}} & 0 & C_{y_{\delta_r}} \\ 0 & C_{z_{\delta_e}} & 0 \end{bmatrix}$$

$$d_V \triangleq \begin{bmatrix} T_{max}/m & 0 & 0 \end{bmatrix}^T$$

$$\begin{aligned} f_R(X) &= (f_{R_1} + f_{R_2} f_{R_3} f_{R_5}) \\ g_R(X) &= f_{R_2} f_{R_3} f_{R_4} \end{aligned}$$

$$f_{R_1} \triangleq \begin{bmatrix} c_1QR + c_2PQ \\ c_5PR + c_6(R^2 - P^2) \\ c_8PQ - c_2QR \end{bmatrix} \quad f_{R_2} \triangleq \bar{q}S \begin{bmatrix} c_3 & 0 & c_4 \\ 0 & c_7 & 0 \\ c_4 & 0 & c_9 \end{bmatrix}$$

$$f_{R_3} \triangleq \begin{bmatrix} b & 0 & 0 \\ 0 & c & 0 \\ 0 & 0 & b \end{bmatrix} \quad f_{R_4} \triangleq \begin{bmatrix} C_{l_{\delta_a}} & 0 & C_{l_{\delta_r}} \\ 0 & C_{m_{\delta_e}} & 0 \\ C_{n_{\delta_a}} & 0 & C_{n_{\delta_r}} \end{bmatrix}$$

$$f_{R_5} \triangleq \begin{bmatrix} C_l(\alpha, \beta) + C_{l_p}(\alpha)\tilde{p} + C_{l_r}(\alpha)\tilde{r} \\ C_m(\alpha) + C_{m_q}(\alpha)\tilde{q} \\ C_n(\alpha, \beta) + C_{n_p}(\alpha)\tilde{p} + C_{n_r}(\alpha)\tilde{r} \end{bmatrix}$$

The longitudinal acceleration n_x, lateral acceleration n_y and normal acceleration n_z are defined as

$$n_x \triangleq (F_x/m) = QW - RV + g\sin\Theta + \dot{U} \quad (30)$$

$$n_y \triangleq (F_y/m) = UR - WP - g\sin\Phi\cos\Theta + \dot{V} \quad (31)$$

$$n_z \triangleq -(F_z/m) = UQ - VP + g\cos\Phi\cos\Theta - \dot{W} \quad (32)$$

Alternately, these quantities can also be written as

$$n_x = f_{n_x} + g_{n_x}U_A \quad (33)$$

$$n_y = f_{n_y} + g_{n_y}U_A \quad (34)$$

$$n_z = f_{n_z} + g_{n_z}U_A \quad (35)$$

where the terms $f_{n_x}, f_{n_y}, f_{n_z}, g_{n_x}, g_{n_y}, g_{n_z}$ are appropriately defined.

Also note that from equations (28) and (29) one can write

$$\dot{V}_T = f_{V_T}(X) + \begin{bmatrix} g_{V_T}(X) & d_{V_T} \end{bmatrix} \begin{bmatrix} U_A \\ \sigma_T \end{bmatrix} \tag{36}$$

$$\dot{P} = f_P(X) + g_P(X)U_A \tag{37}$$

$$\dot{Q} = f_Q(X) + g_Q(X)U_A \tag{38}$$

$$where\, f_{V_T} \triangleq (1/V_T)X_V^T f_V \qquad g_{V_T} \triangleq (1/V_T)X_V^T g_V$$

$$d_{V_T} \triangleq (U/V_T)d_V$$

$$f_P \triangleq f_R(1,:)\ \ g_P \triangleq g_R(1,:)\ \ f_Q \triangleq f_R(2,:)\ \ g_Q \triangleq g_R(2,:)$$

Similarly, in wind axis frame, normal acceleration (n_{wz}) can be written as

$$n_{wz} = f_{n_{wz}} + g_{n_{wz}}U_A \tag{39}$$

where $f_{n_{wz}} = (-sin\alpha\, f_{n_x} + cos\alpha\, f_{n_z})$
$g_{n_{wz}} = (-sin\alpha g_{n_x} + cos\alpha g_{n_z})$

3. FLIGHT CONTROL DESIGN

3.1 Nominal control design

Following the philosophies presented in literature [Kaneshige, Bull & Totah, 2000, Kim & Calise, 1997, Menon, 1993], the objective is to design a controller such that the roll angle $\Phi \to \Phi^*$, normal acceleration $n_z \to n_z^*$, lateral acceleration $n_y \to n_y^*$ and total velocity $V_T \to V_T^*$ where Φ^*, n_z^*, V_T^* are the commanded values from the pilot. $n_y^* = 0$ is preselected in the design process (this assumes turn co-ordination). Note that $\Phi^* = 0$ is also preselected in longitudinal maneuvers. Here we would like to point out that in an available literature [Menon, 1993] n_z^*, n_y^* are typically replaced by proportional and integral error terms in the Command Augmentation System (an outer loop). In this procedure, the required assumptions involved are $\dot{V} = \dot{W} = 0$ and $[\ddot{\Phi}^*\ \ddot{\Theta}^*\ \ddot{\Psi}^*]^T = 0$. Note that since an integral feedback is used, it may lead to"control wind-up", and hence, it is advisable to have an associated wind-up prevention logic (which is not mentioned in the reference). In this paper, however, the need for an intermediate command transformation and the need to introduce any integral feedback for the errors in acceleration commands are eliminated. Moreover, it is assumed that $\ddot{V} = \ddot{W} = 0$, which is a more realistic assumption as compared to assuming $\dot{V} = \dot{W} = 0$. Furthermore, the additional assumption $[\ddot{\Phi}^*\ \ddot{\Theta}^*\ \ddot{\Psi}^*]^T = 0$ is also not necessary. The mathematical details of this new procedure is outlined below in fair detail. First, new variables a_z, a_z^* and a_y, a_y^* are defined as

$$a_z \triangleq n_z + \dot{W}, \quad a_z^* \triangleq n_z^* + \dot{W} \tag{40}$$

$$a_y \triangleq n_y - \dot{V}, \quad a_y^* \triangleq n_y^* - \dot{V} \tag{41}$$

The new method relies on the key observation that $([n_z\ \ n_y]^T \to [n_z^*\ \ n_y^*]^T) \Leftrightarrow ([a_z\ \ a_y]^T \to [a_z^*\ \ a_y^*]^T)$; this is because of the one-to-one correspondence between them. From Equations (31)-(32) and (40)-(41) it can be seen that

$$a_z = UQ - VP + g\cos\Phi\cos\Theta \tag{42}$$

$$a_y = UR - WP - g\sin\Phi\cos\Theta \tag{43}$$

Taking derivatives of both sides with respect to time and using Equations (7)-(9) and (28)-(29), the following equations are obtained,

$$\dot{a}_z = f_{a_z}(X) + \begin{bmatrix} g_{a_z}(X) & d_{a_z} \end{bmatrix} \begin{bmatrix} U_A \\ \sigma_T \end{bmatrix} \tag{44}$$

$$\dot{a}_y = f_{a_y}(X) + \begin{bmatrix} g_{a_y}(X) & d_{a_y} \end{bmatrix} \begin{bmatrix} U_A \\ \sigma_T \end{bmatrix} \tag{45}$$

The symbols used in Equations (44)-(45) are defined below

$$[f_{a_z}(X)\ f_{a_y}(X)]^T \triangleq A_1 f_R(X) + B_1 f_V(X) + C_1 \tag{46}$$

$$[g_{a_z}(X)\ g_{a_y}(X)]^T \triangleq A_1 g_R(X) + B_1 g_V(X) \tag{47}$$

$$[d_{a_z}\ d_{a_y}] \triangleq B_1 d_V \tag{48}$$

where $A_1 \triangleq \begin{bmatrix} -V & U & 0 \\ -W & 0 & U \end{bmatrix}$; $B_1 \triangleq \begin{bmatrix} Q & -P & 0 \\ R & 0 & -P \end{bmatrix}$
$C_1 \triangleq g \begin{bmatrix} -\cos\Theta\sin\Phi & -\cos\Phi\sin\Theta \\ -\cos\Theta\cos\Phi & \sin\Theta\sin\Phi \end{bmatrix} \begin{bmatrix} \dot{\Phi} \\ \dot{\Theta} \end{bmatrix}$

3.1.1. Longitudinal maneuver In the longitudinal maneuver case, goal is to assure that $[\Phi\ n_z\ n_y]^T \to [\Phi^* = 0\ n_z^*\ n_y^* = 0]^T$. However, from Equation (7) it is observed that the control U_A does not appear in the $\dot{\Phi}$ equation. So, we first convert the Φ^* command to the command in roll rate P^*. For doing this, we define the error $\hat{\Phi} \triangleq (\Phi - \Phi^*)$ and enforce a stable desired error dynamics as follows

$$\dot{\hat{\Phi}} + (1/\tau_\Phi)\hat{\Phi} = 0 \tag{49}$$

where $\tau_\Phi > 0$ is the time constant of the error dynamics. By substituting for $\dot{\Phi}$ from Equation (7) and assuming Φ^* to be constant, the desired roll rate (denoted as P^*) is given by the following expression

$$P^* = -(Q\sin\Phi + R\cos\Phi)\tan\Theta - \frac{1}{\tau_\Phi}(\Phi - \Phi^*) \tag{50}$$

where $\tau_\Phi > 0$ is the desired time constant. Next, defining $X_T \triangleq [P\ \ n_z\ \ n_y]^T$, $X_T^* \triangleq [P^*\ \ n_z^*\ \ n_y^* = 0]^T$ and $\hat{X}_T \triangleq (X_T - X_T^*)$, we aim to design a controller such that the following stable linear error dynamics is enforced.

$$\dot{\hat{X}}_T + K\hat{X}_T = 0 \tag{51}$$

where the gain matrix K is selected to be a positive definite matrix. A relatively easier way to select the gain matrix K is to choose the ith diagonal element to be $1/\tau_i$, where $\tau_i > 0$ is the desired time constant of the ith channel of the error dynamics. The gain K is selected as

$$K = diag(1/\tau_P, 1/\tau_{n_z}, 1/\tau_{n_y}) \tag{52}$$

where τ_P, τ_{n_z}, τ_{n_y} are the time constants for roll rate, normal acceleration and lateral error dynamics respectively. With the assumption $\ddot{V} = \ddot{W} = 0$, from Equation (40), it is clear that $[\dot{n}_z \ \dot{n}_y] = [\dot{a}_z \ \dot{a}_y]$. From Equations (37) and (44)-(45), it follows that

$$\begin{bmatrix} f_P + g_P U_A \\ f_{a_z} + g_{a_z} U_A \\ f_{a_y} + g_{a_y} U_A \end{bmatrix} - \dot{X}_T^* \ + \\ K\left(\begin{bmatrix} P \\ f_{n_z} + g_{n_z} U_A \\ f_{n_y} + g_{n_y} U_A \end{bmatrix} - \begin{bmatrix} P^* \\ n_z^* \\ n_y^* \end{bmatrix} \right) = 0 \tag{53}$$

Carrying out necessary algebra, the expression for the controller can be written as

$$U_A = A_U^{-1} b_U \tag{54}$$

where $A_U \triangleq [g_P^T \ g_{a_z}^T \ g_{a_y}^T]^T + K[0^T \ g_{n_z}^T \ g_{n_y}^T]^T$, $b_U \triangleq -[f_P \ f_{a_z} \ f_{a_y}]^T - K[(P-P^*) \ (f_{n_z} - n_z^*) \ (f_{n_y} - n_y^*)]^T$.

Similarly, defining $\hat{V}_T \triangleq (V_T - V_T^*)$ (note that V_T is a slower variable), the following error dynamics is also enforced

$$\dot{\hat{V}}_T + k_{V_T} \hat{V}_T = 0 \tag{55}$$

where the gain matrix $k_{V_T} = 1/\tau_{V_T} > 0$ (where τ_{V_T} is time constant for velocity error dynamics) is selected to be a positive definite matrix. By solving Equation (36) and expression for thrust can be expressed as

$$\sigma_T = -d_{V_T}^{-1} c_{V_T} \tag{56}$$

where $c_{V_T} \triangleq \{(f_{V_T} + g_{V_T} U_A) - \dot{V}_T^* + k_{V_T}(V_T - V_T^*)\}$

Note that the control vector $[\delta_a \ \ \delta_e \ \ \delta_r]$ is updated after every time step dt while σ_T is updated after every five time steps $5dt$ (since it a is slow variable). An implementation schematic of the controller in longitudinal maneuver is given in Figure 1.

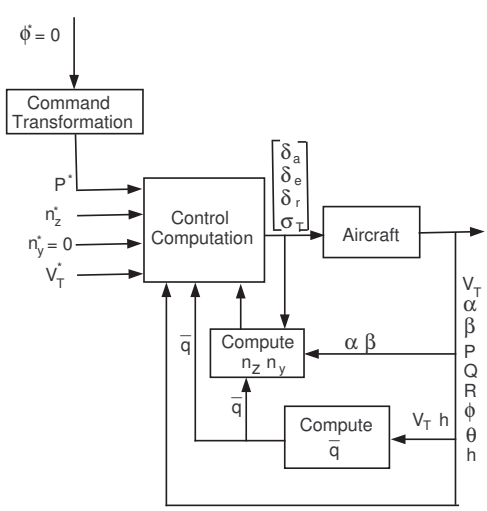

Fig. 1. Implementation of new control design in longitudinal mode

3.1.2. Lateral maneuver During lateral maneuvers, the objectives are to drive $P \to P^*$, $n_y \to n_y^*$, $h \to h^*$ *and* $V_T \to V_T^*$. Note that the appropriate n_z^* (such that $h \to h^*$) is automatically computed in this process. However, from Equation (10) it is observed that the control U_A does not appear in the $\dot{h}$ equation and hence, U_A cannot be computed directly from this goal. Because of this, a command transfer loop is introduced for converting the height command h^* to pitch angle command Θ^*, and subsequently, to the pitch rate command Q^*. In this process, first an error expression is defined as $\hat{h} \triangleq (h - h^*)$ and a stable height-error dynamics is enforced as

$$\dot{\hat{h}} + (1/\tau_h)\hat{h} = 0 \tag{57}$$

where τ_h is the desired time constant for this error dynamics. By substituting for $\dot{h}$ from Equation (10), this can be expanded as

$$[U \sin\Theta - V \cos\Theta \sin\Phi - W \cos\Theta \cos\Phi] \\ -\dot{h}^* + (1/\tau_h)(h - h^*) \ = 0 \tag{58}$$

The variable Θ is solved (denoted as Θ^*) from Equation (58) with a nonlinear equation solver (e.g. Newton-Raphson technique [Gupta, 1995]). Similarly, a stable first-order error dynamics is enforced for the pitch angle dynamics by defining $\hat{\Theta} = (\Theta - \Theta^*)$ and then enforcing the following dynamics.

$$\dot{\hat{\Theta}} + (1/\tau_\Theta)\hat{\Theta} = 0 \tag{59}$$

where $\tau_\Theta > 0$ is the desired time constant. Substituting for $\dot{\Theta}$ equation from Equation (8) and assuming Θ^* to be constant at each instant of time (quasi-steady assumption), an expression for Q (and denote it as Q^*) can be obtained as

$$Q^* = (1/\cos\Phi)[R \sin\Phi - (1/\tau_\Theta)(\Theta - \Theta^*)] \tag{60}$$

The pitch rate Q^* is assumed to be quasi-steady (held constant at each instant of time). Next, define $X_T \triangleq [P \ \ Q \ \ n_y]$, $X_T^* \triangleq [P^* \ \ Q^* \ \ n_y^* = 0]$ and $\hat{X}_T \triangleq (X_T - X_T^*)$. The objective now is to synthesize a controller such that Equation (51) is satisfied. In this case, the gain matrix is selected to be of the form

$$K = diag(1/\tau_P, 1/\tau_Q, 1/\tau_{n_y}) \tag{61}$$

Following the steps outlined before and carrying out the necessary algebra, an expression for control can be written in the following form.

$$U_A = A_U^{-1} b_U \tag{62}$$

where,

$$A_U \triangleq [g_P^T \ g_Q^T \ (g_{a_y}^T + (1/\tau_{n_y}) g_{n_y}^T)]^T$$

$$b_U \triangleq -[f_P \ \ f_Q \ \ f_{a_y}]^T - K[(P - P^*) \ (Q - Q^*) \ (f_{n_y} - n_y^*)]^T$$

σ_T can be calculated by using the same expression as used in Section 3.1.1. Note that the command transformation from h^* to Q^* can be considered as an outer loop, whereas the subsequent control computation can be interpreted as an inner loop. Due to the quasi-steady

assumptions, one should guarantee $\tau_h > \tau_\Theta > \tau_Q$, so that the inner-loop dynamics is faster than the outer-loop dynamics. An implementation schematic of the controller in longitudinal maneuver is given in Figure 2.

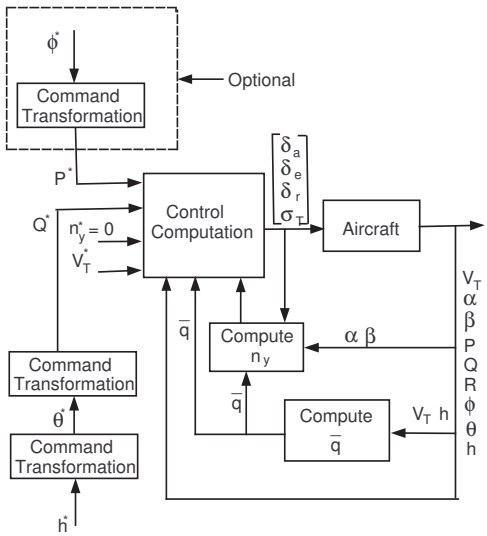

Fig. 2. Implementation of new control design in lateral mode

3.1.3. Combined longitudinal and lateral maneuver

The significance of this maneuver is obvious, for it allows the pilot to quickly slew and point the aircraft's nose using a presumably "fast" roll maneuver, without pulling g's and turning. In this case, goal is $X_T \to X_T^*$ and $V_T \to V_T^*$, where $X_T \triangleq [P \;\; n_z \;\; n_y]^T$, $X_T^* \triangleq [P^* \;\; n_z^* \;\; n_y^* = 0]^T$. Here P_w^* command is given about velocity vector and further P^* is calculated from P_w^*. Using Equations (20), (22) and (23), P^* can be expressed as

$$P^* = f_{P^*} + g_{P^*} U_A \tag{63}$$

where

$$f_{P^*} \triangleq \begin{bmatrix} (1/cos\alpha(cos\beta + tan\beta sin\beta)) \times \\ \left\{ \begin{array}{l} P_w^* - Rsin\alpha(sin\beta tan\beta + cos\beta) \\ -tan\beta((f_{n_{wz}}/V_T) + (g/V_T)cos\gamma cos\Phi) \end{array} \right\} \end{bmatrix}$$

$$g_{P^*} \triangleq (-tan\beta \cos\alpha(cos\beta + tan\beta sin\beta))(g_{n_{wz}}/V_T).$$

Now, a controller is designed such that the stable error dynamics Eq. (51) is satisfied and the gain matrix K is selected to be a positive definite matrix which is taken as same as in Eq. (52). With the assumption $\ddot{V} = \ddot{W} = 0$, from Eq. (40), it is clear that $[\dot{n}_z \;\; \dot{n}_y] = [\dot{a}_z \;\; \dot{a}_y]$. Hence from Eqs. (37), (44) and (45), one can write

$$\begin{bmatrix} f_P + g_P U_A \\ f_{a_z} + g_{a_z} U_A \\ f_{a_y} + g_{a_y} U_A \end{bmatrix} - \dot{X}_T^* + K\left(\begin{bmatrix} P \\ f_{n_z} + g_{n_z} U_A \\ f_{n_y} + g_{n_y} U_A \end{bmatrix} - \begin{bmatrix} f_{P^*} + g_{P^*} U_A \\ n_z^* \\ n_y^* \end{bmatrix} \right) = 0 \tag{64}$$

Simplifying Eq.(64) and carrying out the necessary algebra, the expression for the controller can be derived as

$$U_A = A_U^{-1} b_U \tag{65}$$

where $A_U \triangleq [g_P^T \;\; g_{a_z}^T \;\; g_{a_y}^T]^T + K[-g_{P^*}^T \;\; g_{n_z}^T \;\; g_{n_y}^T]^T$ $b_U \triangleq -[f_P \;\; f_{a_z} \;\; f_{a_y}]^T - K[(P - f_{P^*}) \;\; (f_{n_z} - n_z^*) \;\; (f_{n_y} - n_y^*)]^T$ σ_T can be calculated with the same expression as in Section 3.1.1. An implementation schematic of the controller in combined mode is given in Figure 3.

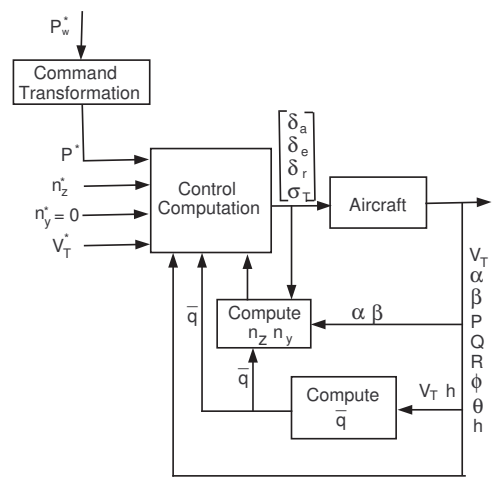

Fig. 3. Implementation of new control design in combined mode

Note that in the dynamic inversion design, the dynamics of the output tracking error is always guaranteed to be globally asymptotically stable (because of the enforcement of stable linear dynamics). But in general there arises the issue of stability of internal dynamics. Even though its difficult to show the stability of internal dynamics analytically using the complicated nonlinear six-DOF equation, from our numerous simulation studies we have observed that the design approach proposed here does not lead to the instability of internal dynamics.

3.2 Neuro-adaptive control design

3.2.1. Generic theory In this approach, as we pointed out earlier the first aim is to come up with a nominal controller, which will meet the goals for the nominal model. The class of nonlinear system is focused on, which can be represented by the following equation

$$\dot{X}_d = f_d(X_d) + G_d(X_d)U_d \tag{66}$$

$$Y_d = h_d(X_d) \tag{67}$$

where $X_d \in \mathbb{R}^n$ and $U_d \in \mathbb{R}^m$, $Y_d \in \mathbb{R}^p$ are the state and control variables of the nominal system respectively. The objective here is to design a controller U_d so that $Y_d \to Y_d$, where $Y_d(t)$ is the commanded signal, which is assumed to be bounded and smooth. The nominal controller U_d has been designed using dynamic inversion technique. Equation (68) may not truly represent

the actual plant because of the presence of uncertainties in the model. Using the chain rule of derivative, the expression for $\dot{Y}$ can be derived as:

$$\dot{Y}_d = f_{Y_d}(X_d) + G_{Y_d}(X_d)U_d \tag{68}$$

where $f_{Y_d} \triangleq [\partial h/\partial X_d] f_d(X_d)$ & $G_{Y_d} \triangleq [\partial h/\partial X_d] G_d(X_d)$. Now the actual plant output is represented as

$$\dot{Y} = f_Y(X) + G_Y(X)U + d_Y(X) \tag{69}$$

$d_Y(X)$ is an unknown function that arises due to parameter uncertainties and unknown disturbances. The controller U needs to be designed online such that the states of the actual plant follow the respective states of the nominal model. In other words, the goal is to ensure that $Y \rightarrow Y_d$ as $t \rightarrow \infty$. To achieve this, the idea followed here is to first capture the unknown function $d_Y(X)$, which is accomplished through a neural network approximation. For this purpose, an intermediate step is needed, which is to define an *approximate system* as follows

$$\begin{aligned} \dot{Y}_a &= f_Y(X) + G_Y(X)U + \hat{d}_Y(X) + K_a(Y - Y_a) \\ Y_a(0) &= Y(0) \end{aligned} \tag{70}$$

where K_a is selected as a positive definite gain matrix. A relatively easy way of doing this is to select K_a as a diagonal matrix with the ith element being $k_{a_i} > 0$. Even though the selection of $k_{a_i} > 0 \ \forall \ i = 1, \ldots, n$ satisfies the need of the k_a being positive definite, it is desirable to choose $k_{a_i} > 1.5$ because it leads to a smaller bound in the tracking error (this will become clear towards the end of this section). Note that whenever a function is approximated and only the approximate function is kept in the dynamics, then the modified equation no more represents the true dynamics (because of the function approximation error). This is the primary reason to introduce the Y_a dynamics. The approach followed here for ensuring $Y \rightarrow Y_d$ involves two steps: (i) $Y \rightarrow Y_a$ and (ii) $Y_a \rightarrow Y_d$, which are discussed next. A pictorial representation of these steps is shown in the Fig.4.

Step1 Capturing $d_Y(X)$ and ensuring $Y \rightarrow Y_a$. To

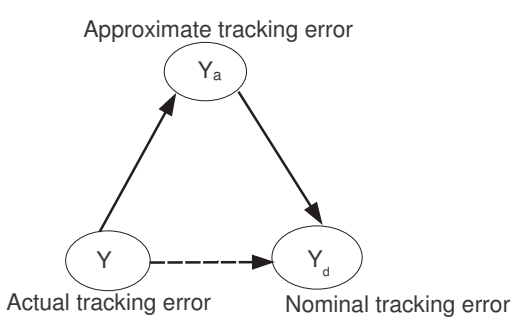

Fig. 4. Philosophy of model following approach

capture the unknown function, first write $d_Y(X) \triangleq \left[d_{Y_1}(X) \ \ldots \ d_{Y_n}(X) \right]$ where $d_{Y_i}(X), i = 1, 2, \ldots . n$ is the ith component of the $d_Y(X)$. Each $d_Y(X)$ is approximated as $\hat{d}_Y(X)$ in a separate linear-in-the-weight neural network. We assume that the unknown function $d_Y(X)$ can be represented by the basis function vector $\phi(X)$

$$\hat{d}_{Y_i}(X) = \hat{W}_i^T \phi_i(X) \tag{71}$$

where $\hat{W}_i$ is the weight vector of the ith neural network and $\phi_i(X)$ is its basis function vector for each channel. This neural network function approximation is depicted in Fig. 5.

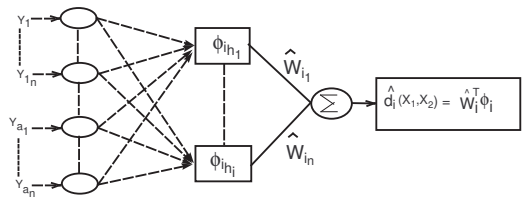

Fig. 5. Linear-in-weight neural network

At this point, it needs to be mentioned that even though generic radial basis functions can be used for this purpose. It is probably wiser to incorporate some prior knowledge about the system and judiciously select the basis functions, which will lead to faster learning of the unknown function. Note that the combination of n sub-networks can be interpreted to constitute a single neural network that represents $d_Y(X)$. The idea of having n neural networks for n independent channels is to facilitate simpler mathematical analysis. More important, it leads to faster training because of reduced computational complexity, as none of the weights are linked to more than one output function. The next task is to update the weights of the neural network (i.e. to train them). Towards this end, the error between the actual state and the corresponding approximate state is defined as

$$e_{ai} \triangleq Y_i - Y_{ai} \tag{72}$$

From Eq. (69) and Eq. (70), the equations for the ith channel e_{ai} is written as

$$\begin{aligned} \dot{e}_{a_i} &\triangleq d_{Y_i}(X) - \hat{d}_{Yi}(X) - k_{a_i i} e_{ai} \\ &= \tilde{W}^T{}_i \phi_i(X) + \varepsilon_i - k_{ai} e_{ai} \end{aligned} \tag{73}$$

where $\tilde{W} \triangleq (W_i - \hat{W})$ is the error between the ideal weight and actual weight of the neural network. Next,define a series of Lyapunov function candidates $L_i, i = 1, 2, \ldots n$ such that

$$L_i = \frac{e_{ai} p_i e_{ai}}{2} + \frac{\tilde{W}_i^T \gamma_i^{-1} \tilde{W}_i}{2} \tag{74}$$

where $p_i > 0$ and $\gamma_i > 0$. Taking the time derivative of both sides of Eq. (74), using the fact that $\dot{\tilde{W}} = -\dot{\hat{W}}_i$ (Since W_i is a constant) and on substituting for $\dot{e}_{ai}$ from Eq. (74)

$$\begin{aligned}\dot{L}_i &= e_{ai}p_i\dot{e}_{a_i} + \tilde{W}_i^T\gamma_i^{-1}\dot{\tilde{W}}_i \\ &= e_{ai}p_i(\tilde{W}_i^T\phi_i(X) + \varepsilon_i - k_{a_i}e_{ai}) + \tilde{W}_i^T\gamma_i^{-1}\dot{\tilde{W}}_i\end{aligned} \tag{75}$$

Note that our objective is to come up with a meaningful condition that will ensure $\dot{L}_i < 0$ which will ensure the stability of the error dynamics (of tracking error as well as weight error). However, the expression for $\dot{L}_i$ contains $\tilde{W}_i$ (which is unknown), and hence, nothing can be concluded about the sign of $\dot{L}_i$. To get rid of this difficulty, force the term multiplying it to zero and obtain the following weight update rule (training algorithm) for the ith neural network.

$$\dot{\hat{W}}_i = \gamma_i e_{ai}p_i\phi_i(X) - \sigma_i\gamma_i\hat{W}_i \tag{76}$$

where γ_i can be interpreted as a learning rate for the ith network (its numerical value essentially dictates the rate of capturing the unknown function) $d_{Y_i}(X)$. Note that Eq. (76) is the weight update (learning) rule for $\tilde{W}_i$. Select the initial condition as $\tilde{W}_i(0) = 0$. This is compatible with the fact that if $d_{Y_i}(X) = 0$ (i.e. there is no error in the model), then automatically $\hat{d_{Y_i}}(X) = 0$. From the previous discussion we know that $\dot{\tilde{W}}_i = -\dot{\hat{W}}_i$, therefore Eq. (75) becomes

$$\dot{L}_i = e_{ai}p_i(\tilde{W}_i^T\phi_i(X) + \varepsilon_i - k_{ai}e_{ai}) - \tilde{W}_i^T\gamma_i^{-1}\dot{\hat{W}}_i \tag{77}$$

Substituting $\dot{e_{a_i}}$ from Eq. (73) and $\dot{\hat{W}}_i$ from Eq. (76) in Eq. (77), we get

$$\dot{L}_i = e_{a_i}p_i\varepsilon_i - k_{a_i}e_{a_i}^2p_i + \sigma_i\tilde{W}_i^T\hat{W}_i \tag{78}$$

However $\tilde{W}_i^T\hat{W}_i$, the last term from Eq. (78) can be derived as follows

$$\tilde{W}_i^T\hat{W}_i = \frac{2}{2}\left(\tilde{W}_i^T\hat{W}_i\right) = \frac{1}{2}\left(2\tilde{W}_i^TW_i - 2\tilde{W}_i^T\tilde{W}_i\right) \tag{79}$$

Further expanding $2\tilde{W}_i^TW_i$, the first term from Eq.(79) becomes

$$\begin{aligned}2\tilde{W}_i^TW_i &= \tilde{W}_i^TW_i + \tilde{W}_i^TW_i \\ &= \tilde{W}_i^T\left(\hat{W}_i + \tilde{W}_i\right) + \left(W_i - \hat{W}_i\right)^TW_i \\ &= \hat{W}_i^T\left(\tilde{W}_i - W_i\right) + \tilde{W}_i^T\tilde{W}_i + W_i^TW_i \\ &= -\hat{W}_i^T\hat{W}_i + \tilde{W}_i^T\tilde{W}_i + W_i^TW_i\end{aligned} \tag{80}$$

Using Eq. (80), Eq. (79) can be expressed as

$$\begin{aligned}\tilde{W}_i^T\hat{W}_i &= \frac{1}{2}\begin{pmatrix}-\hat{W}_i^T\hat{W}_i + \tilde{W}_i^T\tilde{W}_i \\ +W_i^TW_i - \tilde{W}_i^T\tilde{W}_i - \tilde{W}_i^T\tilde{W}_i\end{pmatrix} \\ &\leq \frac{1}{2}\left(-\|\tilde{W}_i\|^2 - \|\hat{W}_i\|^2 + \|W_i\|^2\right)\end{aligned} \tag{81}$$

Therefore the last term in Eq. (78) satisfies the following inequality

$$\sigma_i\tilde{W}_i^T\hat{W}_i \leq -\frac{1}{2}\sigma_i\|\tilde{W}_i\|^2 - \frac{1}{2}\sigma_i\|\hat{W}_i\|^2 + \frac{1}{2}\sigma_i\|W_i\|^2 \tag{82}$$

Equation (78) can now be rewritten as

$$\begin{aligned}\dot{L}_i \leq\ & e_{a_i}p_i\varepsilon_i - e_{a_i}^2p_ik_{a_i} - \frac{1}{2}\sigma_i\|\tilde{W}_i\|^2 \\ & -\frac{1}{2}\sigma_i\|\hat{W}_i\|^2 + \frac{1}{2}\sigma_i\|W_i\|^2 \\ \leq\ & \frac{e_{a_i}^2p_i}{2} + \frac{\varepsilon_i^2p_i}{2} - e_{a_i}^2p_ik_{a_i} - \frac{1}{2}\sigma_i\|\tilde{W}_i\|^2 \\ & -\frac{1}{2}\sigma_i\|\hat{W}_i\|^2 + \frac{1}{2}\sigma_i\|W_i\|^2 \\ \leq\ & \frac{e_{a_i}^2p_i}{2} + \frac{\varepsilon_i^2p_i}{2} - \frac{1}{2}\sigma_i\|\tilde{W}_i\|^2 \\ & -\frac{1}{2}\sigma_i\|\hat{W}_i\|^2 + \frac{1}{2}\sigma_i\|W_i\|^2\end{aligned} \tag{83}$$

In the expression 83, $\dot{L}_i < 0$ is only possible if $\frac{e_{a_i}}{2} > \beta_i$ or $|e_{a_i}| > \sqrt{2\beta_i}$ where
$\beta_i \triangleq \left[\frac{\varepsilon_i^2p_i}{2} - \frac{1}{2}\sigma_i\|\tilde{W}_i\|^2 - \frac{1}{2}\sigma_i\|\hat{W}_i\|^2 + \frac{1}{2}\sigma_i\|W_i\|^2\right]$.

Thus, it is evident that by selecting a small σ_i and sufficiently good set of basis functions, the approximation error ε_i will be reduced, which will help in keeping the error bound small.

Step2 Ensuring $Y_a \rightarrow Y_d$ and Computation of U

As pointed out earlier, while ensuring $Y \rightarrow Y_a$ and capturing the unknown function $d_Y(X)$ as a functional approximation $\hat{d_Y}(X)$, it is simultaneously ensured that $Y_a \rightarrow Y_d$ as $t \rightarrow \infty$. To achieve this objective, the controller U is designed such that the following stable error dynamics is satisfied

$$(\dot{Y}_a - \dot{Y}_d) + K_g(Y_a - Y_d) = 0 \tag{84}$$

where K_g is chosen to be a positive definite gain matrix. A relatively easy way of choosing the gain matrix is to have $K_g = diag(1/\tau_1 \ldots 1/\tau_n)$, where τ_i can be interpreted as the desired time constant for the ith channel of the error dynamics in Eq. (84). From Eq. (68) and Eq. (70) and carrying out necessary algebra, the adaptive control is obtained as

$$U = -G_{Y_d}^{-1}\begin{bmatrix} f_Y + \hat{d_Y}(X) + K_a(Y - Y_a) - \\ f_Y(X_d) - G_Y(X_d)U_d + \\ K(Y_a - Y_d)\end{bmatrix} \tag{85}$$

Note that even though we have used this technique in conjunction with dynamic inversion, the generic neuro-adaptive control design presented in this section can be implemented with 'any' baseline controller to make it robust with respect to parametric and modeling inaccuracies.

3.2.2. Problem specific equations For longitudinal as well as lateral modes, first a nominal controller was designed using dynamic inversion technique as described earlier. Then randomness was introduced by assuming Gaussian distributions around the nominal parameter values (which were considered as the mean value of the distribution). The uncertain parameters (mass, moment of inertia and aerodynamic

coefficients) are varied at random using Gaussian distribution from 1% *to* 3%. A 3σ spread was assumed to cater to this distribution of the data and numbers were generated from this distribution at random. Note that even though the system dynamics was simulated with these random values, this information was not used in the control design (i.e. in the control design only nominal values of the parameters were used). Next a neuro-adaptive controller was designed using the technique described earlier.

Longitudinal maneuver In longitudinal mode the output vector is

$$Y(X) = [\phi \; n_z \; n_y \; V_T]^T \tag{86}$$

But as the control does not appear in the $\dot{\phi}$ equation, a command transformation is done and the output dynamics is written as follows

$$\dot{Y}(X) = [\dot{P} \; \dot{a}_z \; \dot{a}_y \; V_T]^T \tag{87}$$

The first three output dynamics are dealt together and the fourth one, which ultimately gives the solution for the thrust (which is a slow variable) is handled separately.

In this problem, the error equation is given by

$$\begin{bmatrix} \dot{P}_a \\ \dot{a}_{z_a} \\ \dot{a}_{y_a} \\ \dot{V}_{T_a} \end{bmatrix} - \begin{bmatrix} \dot{P}_d \\ \dot{a}_{z_d} \\ \dot{a}_{y_d} \\ \dot{V}_{T_d} \end{bmatrix} + K \left(\begin{bmatrix} P_a - P_d \\ n_{z_a} - n_{z_d} \\ n_{y_a} - n_{y_d} \\ V_{T_a} - V_{T_d} \end{bmatrix} \right) = 0 \tag{88}$$

Substituting the relevant expressions, 88 can be written as

$$\begin{bmatrix} f_{P_a} \\ f_{a_{z_a}} \\ f_{a_{y_a}} \\ f_{V_{T_a}} \end{bmatrix} + \begin{bmatrix} g_{P_a} & 0 \\ g_{a_{z_a}} & d_{a_{z_a}} \\ g_{a_{y_a}} & d_{a_{y_a}} \\ g_{V_{T_a}} & d_{V_{T_a}} \end{bmatrix} \begin{bmatrix} U_{A_a} \\ \sigma_{T_a} \end{bmatrix} + K \begin{bmatrix} P_a - P_d \\ n_{z_a} - n_{z_d} \\ n_{y_a} - n_{y_d} \\ V_{T_a} - V_{T_d} \end{bmatrix} + \begin{bmatrix} \hat{d}_P \\ \hat{d}_{a_z} \\ \hat{d}_{a_y} \\ \hat{d}_{V_T} \end{bmatrix} + K_a \begin{bmatrix} P - P_a \\ n_z - n_{z_a} \\ n_y - n_{y_a} \\ V_T - V_{T_a} \end{bmatrix} = 0 \tag{89}$$

From, 89 the control can be obtained as below

$$\begin{bmatrix} U_{A_a} \\ \sigma_{T_a} \end{bmatrix} = \begin{bmatrix} g_{P_a} & o \\ g_{a_{z_a}} & d_{a_{z_a}} \\ g_{a_{y_a}} & d_{a_{y_a}} \\ g_{V_{T_a}} & d_{V_{T_a}} \end{bmatrix}^{-1} + \begin{bmatrix} f_{P_d} \\ f_{a_{z_d}} \\ f_{a_{yd}} \\ f_{V_{T_d}} \end{bmatrix} + \begin{bmatrix} g_{P_d} & o \\ g_{a_{z_d}} & d_{a_{z_d}} \\ g_{a_{y_d}} & d_{a_{y_d}} \\ g_{V_{T_d}} & d_{V_{T_d}} \end{bmatrix} \begin{bmatrix} U_{A_d} \\ \sigma_{T_d} \end{bmatrix} - \begin{bmatrix} \hat{d}_P \\ \hat{d}_{a_z} \\ \hat{d}_{a_y} \\ \hat{d}_{V_T} \end{bmatrix} - \begin{bmatrix} f_{P_a} \\ f_{a_{za}} \\ f_{a_{ya}} \\ f_{V_{Ta}} \end{bmatrix} - K \begin{bmatrix} P_a - P_d \\ n_{z_a} - n_{z_d} \\ n_{y_a} - n_{y_d} \\ V_{T_a} - V_{T_d} \end{bmatrix} - K_a \begin{bmatrix} P - P_d \\ n_z - n_{z_d} \\ n_y - n_{y_d} \\ V_T - V_{T_d} \end{bmatrix}$$

Lateral maneuver In lateral mode the output vector is

$$Y(X) = [\phi \;\; h \;\; n_y \;\; V_T]^T \tag{90}$$

But as the control does not appear in the $\dot{\phi}$ equation, a command transformation is done and the output dynamics is written as follows

$$\dot{Y}(X) = [\dot{P} \;\; \dot{Q} \;\; \dot{a}_y \;\; V_T]^T \tag{91}$$

The first three output dynamics are dealt together and the fourth one, which ultimately gives the solution for the thrust (which is a slow variable) is handled separately.

In this problem, the error equation is given by

$$\begin{bmatrix} \dot{P}_a \\ \dot{Q}_a \\ \dot{a}_{y_a} \\ \dot{V}_{T_a} \end{bmatrix} - \begin{bmatrix} \dot{P}_d \\ \dot{Q}_d \\ \dot{a}_{y_d} \\ \dot{V}_{T_d} \end{bmatrix} + K \left(\begin{bmatrix} P_a - P_d \\ Q_a - Q_d \\ n_{y_a} - n_{y_d} \\ V_{T_a} - V_{T_d} \end{bmatrix} \right) = 0 \tag{92}$$

Substituting the relevant expressions, 92 can be written as

$$\begin{bmatrix} f_{P_a} \\ f_{Q_a} \\ f_{a_{ya}} \\ f_{V_{Ta}} \end{bmatrix} + \begin{bmatrix} g_{P_a} & 0 \\ g_{Q_a} & d_{Q_a} \\ g_{a_{ya}} & d_{a_{ya}} \\ g_{V_{Ta}} & d_{V_T} \end{bmatrix} \begin{bmatrix} U_{A_a} \\ \sigma_{T_a} \end{bmatrix} + K \begin{bmatrix} P_a - P_d \\ Q_a - Q_d \\ n_{y_a} - n_{y_d} \\ V_{T_a} - V_{T_d} \end{bmatrix} + \begin{bmatrix} \hat{d}_P \\ \hat{d}_Q \\ \hat{d}_{a_y} \\ \hat{d}_{V_T} \end{bmatrix} + K_a \begin{bmatrix} P - P_a \\ Q - Q_a \\ n_y - n_{y_a} \\ V_T - V_{T_a} \end{bmatrix} = 0 \tag{93}$$

From , 93 the control can be obtained as below

$$\begin{bmatrix} U_{A_a} \\ \sigma_{T_a} \end{bmatrix} = \begin{bmatrix} g_{P_a} & 0 \\ g_{Q_a} & d_{Q_a} \\ g_{a_{ya}} & d_{a_{y_a}} \\ g_{V_{T_a}} & d_{V_{T_a}} \end{bmatrix}^{-1} + \begin{bmatrix} f_{P_d} \\ f_{Q_d} \\ f_{a_{yd}} \\ f_{V_{T_d}} \end{bmatrix} + \begin{bmatrix} g_{P_d} & 0 \\ g_{Q_d} & d_{Q_d} \\ g_{a_{y_d}} & d_{a_{y_d}} \\ g_{V_{T_d}} & d_{V_{T_d}} \end{bmatrix} \begin{bmatrix} U_{A_d} \\ \sigma_{T_d} \end{bmatrix} - \begin{bmatrix} \hat{d}_P \\ \hat{d}_Q \\ \hat{d}_{a_y} \\ \hat{d}_{V_T} \end{bmatrix} - \begin{bmatrix} f_{P_a} \\ f_{Q_a} \\ f_{a_{ya}} \\ f_{V_{Ta}} \end{bmatrix} - K \begin{bmatrix} P_a - P_d \\ Q_a - Q_d \\ n_{y_a} - n_{y_d} \\ V_{T_a} - V_{T_d} \end{bmatrix} - K_a \begin{bmatrix} P - P_d \\ Q - Q_d \\ n_y - n_{y_d} \\ V_T - V_{T_a} \end{bmatrix}$$

A necessity in the process of neural network training is to choose appropriate basis functions. Trying to retain the generic nature of this problem, the basis functions are chosen as Gaussian functions. The basis function vector in each channel is chosen as follows

$$\varphi_i(X) = \begin{bmatrix} e^{-\frac{1}{2}\left(\frac{(y_i - y_{ia})^2}{\sigma_1^2}\right)} \\ e^{-\frac{1}{2}\left(\frac{(y_i - y_{ia})^2}{\sigma_2^2}\right)} \\ e^{-\frac{1}{2}\left(\frac{(y_i - y_{ia})^2}{\sigma_3^2}\right)} \end{bmatrix}$$

For better approximation, we have selected three Gaussian basis functions about each of the mean val-

ues as $\sigma_1 = 0.1$ $\sigma_2 = 1$ $\sigma_3 = 10$. Note that the selection of Gaussian functions as the basis functions is in accordance with the universal function approximation theory of neural networks. The initial conditions of the neural network weights were assumed to be zero.

3.3 Actuator dynamics

Actuators for the control surface and engine are modeled as first order lags with limits on their minimum and maximum values as well as their rates. The magnitude and rate limits, as well as time constants of the actuators used in the nonlinear aircraft model are shown in Table 3.

4. NUMERICAL EXPERIMENTS

4.1 Numerical data selection

The low fidelity aerodynamic model data, as well as the Moment-of-Inertia data, for the F-16 aircraft is used in our simulation study [Nguyen et al., 1979]. A fourth-order Runge-Kutta technique [Gupta, 1995] with fixed step size of 50 msec is used for numerical integration, which was motivated from [Keviczky & Balas, 2006]

4.1.1. Trim condition The trim condition for steady level flight is calculated by minimizing the following cost function (J) with specified initial velocity and altitude [Russell, 2003].

$$J = 5\dot{h}^2 + 10\dot{\Phi}^2 + 10\dot{\Theta}^2 + 10\dot{\Psi}^2$$
$$+2\dot{V_T}^2 + 10\dot{\alpha}^2 + 10\dot{\beta}^2 + 10\dot{P}^2 + 10\dot{Q}^2 + 10\dot{R}^2$$

The cost function is minimized by the Matlab's function *fminsearch*, which finds values for the free parameters by using an iterative technique. The trim condition values (as found by minimizing (J)) at specified velocity $V_{T_0} = 580\ (ft/sec)$ and altitude $h_0 = 10,000\,ft$ are given in Table 1.

4.1.2. Selection of control design parameters

Nominal control design After some trial and error tuning, the values selected for the time constants (design parameters) are given in Table 2. Note that the some of these time constant values are not required in the longitudinal mode whereas τ_{n_z} value is not necessary in the lateral mode. Also note that the numerical values of the design parameters are kept same in both the modes, which facilitates easier implementation (especially in the combined longitudinal and lateral mode).

In order to compare the performance of the new control design method proposed here with an existing version [Menon, 1993] (see appendix for a summary of it), gain values of $k_1 = k_3 = 1, \quad k_2 = k_4 = 30$ were selected for the command augmentation system. Similarly in the attitude orientation system, parameter values of $k_{v_i} = 2\zeta_i\omega_{n_i},\ \ k_{p_i} = \omega_{n_i}^2$ with $\zeta_1 = 1.5,\ \ \zeta_2 = 0.9,\ \ \zeta_3 = 0.9$ and $\omega_1 = 2,\ \ \omega_2 = 5,\ \ \omega_3 = 5$ rad/sec $(i = 1,2,3)$ were selected for each of the attitude angle error dynamic channels and the time constants for this case as well. It is important to point out that the existing technique need eleven design parameters in the longitudinal case and twelve design parameters in the lateral case. In the new approach presented in this study, however only five design parameters are needed for the longitudinal mode and seven parameters are required for the lateral case. This significantly less number of design parameters with better performance is clearly a potential advantage of the new approach.

Adaptive control design The learning rate for the longitudinal and lateral mode is 60 except for the total velocity in the lateral mode which is 40. The scalar selected for longitudinal mode is $P_p = 0.0001,\ \ P_{n_z} = 0.05,\ \ P_{n_y} = 0.001,\ \ P_{V_T} = 0.005$. And for the lateral mode it is $P_p = P_q = P_{n_y} = 0.0001,\ \ P_{V_T} = 0.05$. The gains and for the longitudinal mode are given as $K = diag(5,\ 5,\ 5,\ 4)$, and $K_a = diag(0.05,\ 0.05,\ 0.05,\ 1)$. The gains selected for the lateral mode are $K = diag(5,\ 4,\ 4,\ 4)$, and $K_a = diag(0.05,\ 0.8,\ 0.05,\ 0.05)$.

4.2 Analysis of results

4.2.1. Nominal control design In the representative numerical results presented here, the goal is to track the reference commands for 90 sec in longitudinal case and 60 sec in lateral case. Within this time slot, the command is altered to reflect possible real-life scenarios. In all plots (Figures 6 - 17), the solid lines represent the results from the new approach presented in this report, whereas the dashed lines represent the results from the existing approach [Menon, 1993].

Longitudinal maneuver In Figures 6 - 9, simulation results for a longitudinal maneuver are shown, starting from the trim condition. The upper value of n_z^* assumed for low-fidelity model of F-16 [Keviczky & Balas, 2006] is 2.0g. The following sequence of command signals is input: $[\Phi^* \quad n_y^* \quad V_T^*] = [0 \quad 0 \quad V_{T_0}]$ throughout the maneuver, $n_z^* = 0.9965g$ for $t = (0-1)$ sec, $2.0g$ for $t = (1-15)$ sec, $0.5g$ for $t = (15-65)$ sec, $1.0g$ for $t = (65-90)$ sec.

In Figure 6, it is clear that the goal of normal acceleration tracking is met for both approaches. However,

Table 1. *Trim Condition Values*

Parameter	α_0	β_0	Φ_0	Θ_0	Ψ_0	δ_{a_0}	δ_{e_0}	δ_{r_0}	σ_{T_0}
Trim Value	1.497 deg	0 deg	1.497 deg	0 deg	0 deg	0 deg	-1.81 deg	0 deg	0.09

Table 2. *Time Constant Values (N/R: Not Required)*

Time constant (sec)	τ_P	τ_{n_z}	τ_{n_y}	τ_{V_T}	τ_Φ	τ_Θ	τ_Q	τ_h
Longitudinal	0.3	1.5	2	3	1	N/R	N/R	N/R
Lateral	0.3	N/R	2	3	1	0.3	0.1	5

Table 3. *Engine and Control surface actuator's description*

	$Engine(throttle)$	$Elevator$	$Aileron$	$rudder$
upper level limit	19000 lb	+25 deg	+21.5 deg	+30 deg
lower level limit	1000 lb	-25 deg	-21.5 deg	-30 deg
upper rate limit	+10000 lb/s	+60 deg/sec	+80 deg/sec	+120 deg/sec
lower rate limit	-10000 lb/s	-60 deg/sec	-80 deg/sec	-120 deg/sec
time constant	1	0.0495	0.0495	0.0495

the new approach offers several improvements. First, the transient oscillations have much smaller overshoot and the frequency of oscillation is lesser (which is also evident from the normal acceleration and pitch rate history in Figures 6 and 8). This leads to better handling quality of the airplane. From Figure 6, it can also be observed that even though the normal acceleration is eventually tracked in the existing approach [Menon, 1993] successfully, the closed loop shows a non-minimum phase behavior (i.e. the initial response is in the opposite direction with respect to the command before recovering back).

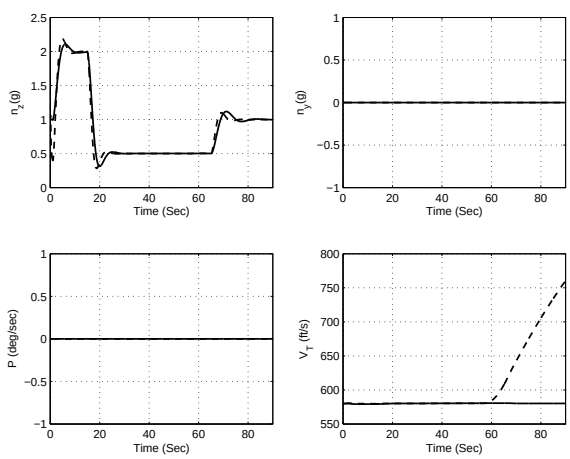

Fig. 6. Roll angle, Normal acceleration, Lateral acceleration and Total velocity in longitudinal maneuver

From Figure 7, it is evident that the control surface deflections are approximately zero in both the approaches (i.e aileron and rudder deflections). However, the final elevator deflection requirement is less in the new approach. Moreover, the existing approach exhibits oscillations of relatively higher frequency in the elevator. The main difference here is that, in existing method thrust saturation starts very early as compared to this new method (which is shown in Figure 7) and it goes below the lower permissible limit of thrust (taken as 1000 lb [Nguyen et al., 1979]). After saturation, the velocity deviates from its desired goal, but in the new method it is able to recover and the desired goal is achieved leading to better tracking.

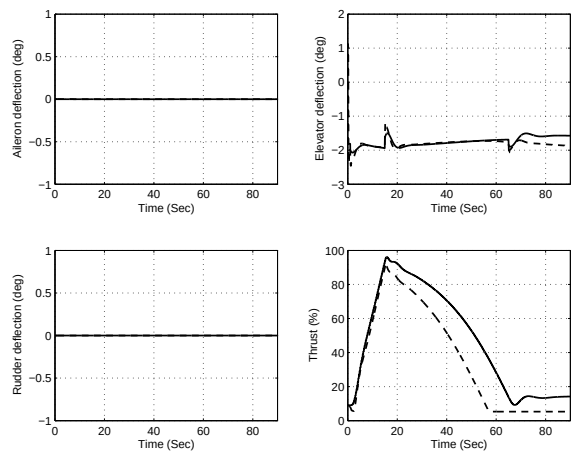

Fig. 7. Aileron, Elevator and Rudder deflections and Thrust level in longitudinal maneuver

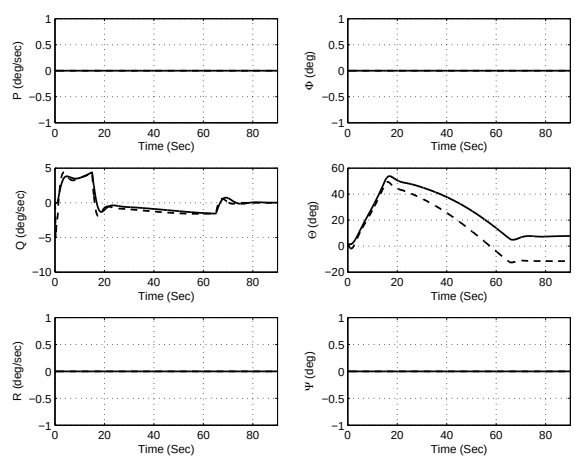

Fig. 8. Roll, Pitch, Yaw rate and Euler angles in longitudinal maneuver

The aerodynamic and state variables are also presented in Figures 8 and 9. It is clear that all the non-tracked state variables remain within reasonable values throughout the maneuver (i.e. the internal dynamics remains stable). Note that even though only one set of representative results are presented here, simulation studies for a large number of cases led to similar advantages and did not show instability in any of the cases.

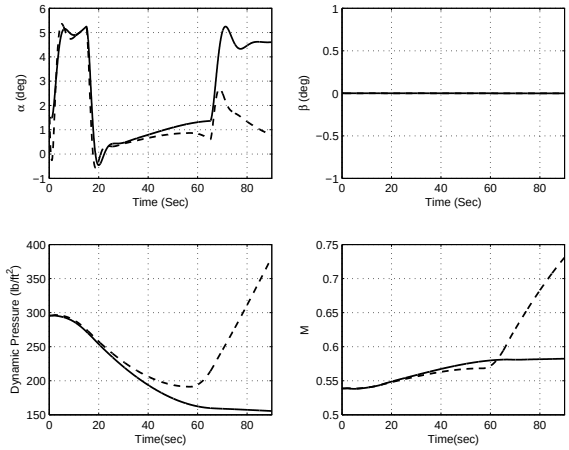

Fig. 9. Aerodynamic variables in longitudinal maneuver

Lateral maneuver Simulation results for a lateral maneuver from the trim condition are presented in Figures 10 - 13. The sequence of command signals applied consists of $P^* = -10\ deg/sec$ for $t = (0-7)$ sec, $P^* = 10\ deg/sec$ for $t = (7-14)$ sec and $P^* = 0\ deg/sec$ for $t = (14-60)$ sec. Throughout the maneuver, it was assumed that $V_T^* = V_{T_0},\ \ h^* = h_0$ (the initial condition values). However, the pilot can essentially select any other reasonable values. From Figure 11, in case of new approach, it is clearly shown that aileron, elevator and rudder deflections are relatively lesser at 7 sec. Besides, in the existing approach the elevator and rudder deflection histories show relatively high magnitude and high frequency transient oscillations, which should preferably be avoided. These trends are absent in the performance of this new approach. From the graph, it is clear that thrust required is also less (around half) as compared to existing method, which is again an advantage. Note that the lateral accelerations in both approaches remain close to zero (which is also evident in small side-slip angle in Figure 13), which was a requirement for the maneuvers. However, in the new approach both side-slip angles remain more closer to zero and oscillations are also relatively lesser. In other words, it leads to better turn-coordination. Pitch rate also more magnitude with more oscillations, which is shown in Figure 12. All other state and aerodynamic variables are also plotted in Figures 12 and 13, they also shows high frequency transient oscillations with more magnitude as compared to this new approach.

In the second case, P^* command is generated using bank angle command as discussed before. In this case, the sequence of command signals applied consisted of $\Phi^* = -40\ deg$ for $t = (0-10)$ sec, $\Phi^* = 40\ deg$ for $t = (10-20)$ sec and $\Phi^* = 0\ deg$ for $t = (20-60)$ sec. Throughout the maneuver it was assumed that $V_T^* = V_{T_\circ},\ \ h^* = h_\circ$ (the initial condition values).

Trajectories of the tracked states and associated controls are presented in Figures 14 - 17. The response plots for the tracked variables (as shown in Figure 14) do not show much of the difference, except that

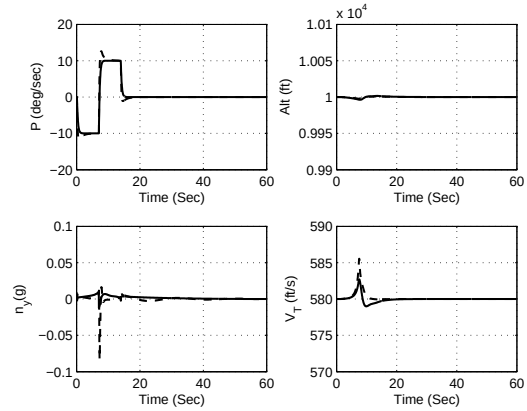

Fig. 10. Roll rate, height, Lateral acceleration and Total velocity in the lateral maneuver

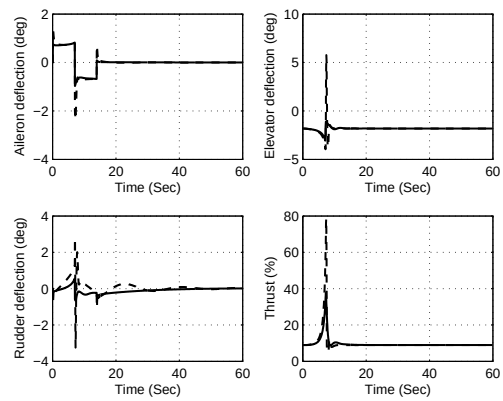

Fig. 11. Aileron, Elevator and Rudder deflections and Thrust level in lateral maneuver

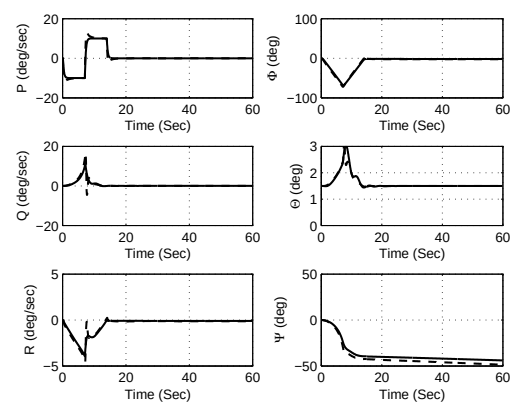

Fig. 12. Roll, Pitch and Yaw rate and Euler angles in lateral maneuver

the n_y deviation is more (about 5 times) in the existing method. However, in Figure 15 it is shown that the magnitudes of the aileron and rudder controllers (main controllers for lateral case) are much lower in the new method whenever the bank angle command is changed. From Figure 16, it is evident that there is sudden increase in the roll rate to about 80 (deg/sec) in the existing approach, which is much higher as compared to the new technique proposed. From a large number of simulation studies it was found that the untracked states remain within reasonable limits.

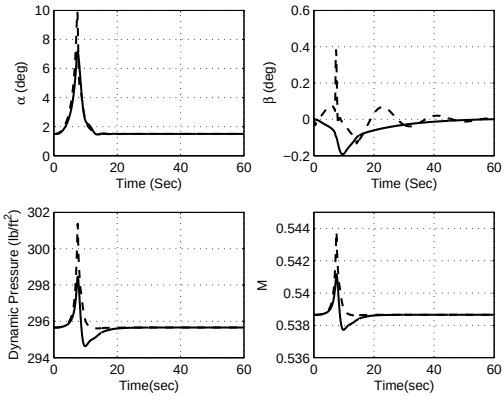

Fig. 13. Aerodynamic variables in lateral maneuver

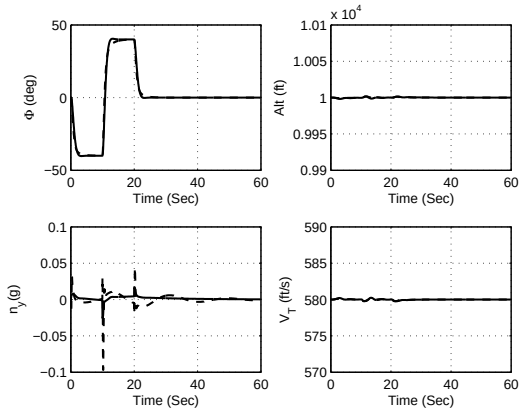

Fig. 14. Roll angle, height, Lateral acceleration and Total velocity in lateral maneuver

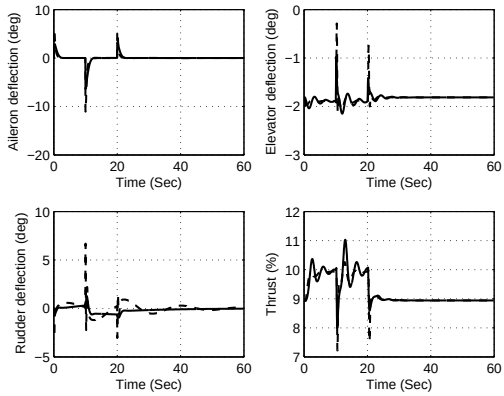

Fig. 15. Aileron, Elevator and Rudder deflections and Thrust level in lateral maneuver

Combined longitudinal and lateral maneuver In many recent literature [Wang & Stengel, 2005, Muir, 1998, Pachter, 1996] velocity vector roll is performed at constant angle of attack, which is predominantly a lateral maneuver but coupled with some longitudinal component as well. This is done to get a faster response from the aircraft. We have also performed such an exercise, by simultaneously giving normal acceleration command (instead of maintaining a constant angle of attack) with the velocity vector roll command. The command set also includes a velocity command

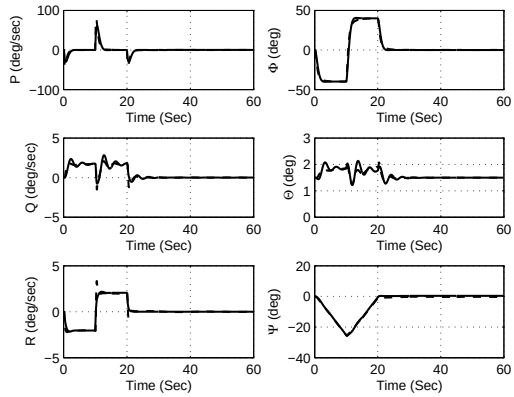

Fig. 16. Roll, Pitch and Yaw rate and Euler angles in lateral maneuver

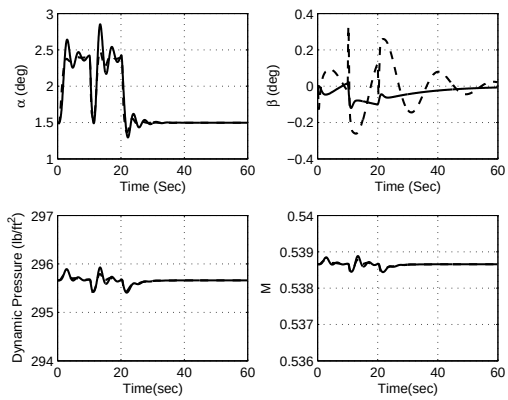

Fig. 17. Aerodynamic variables in lateral maneuver

and the lateral acceleration command (which is zero). Even though this is a difficult task in general, we wish to point out that the approach proposed here works well for this case as well. Simulation results for combined longitudinal and lateral maneuver are presented in Figures 18 - 21. In this maneuver the pilot commands given are normal acceleration, velocity vector roll rate, lateral acceleration and total velocity. Note that promising results have also been obtained with constant angle of attack maneuvers along with velocity vector roll (in lieu of normal acceleration command). However, those results are not presented here to contain the length of the paper.

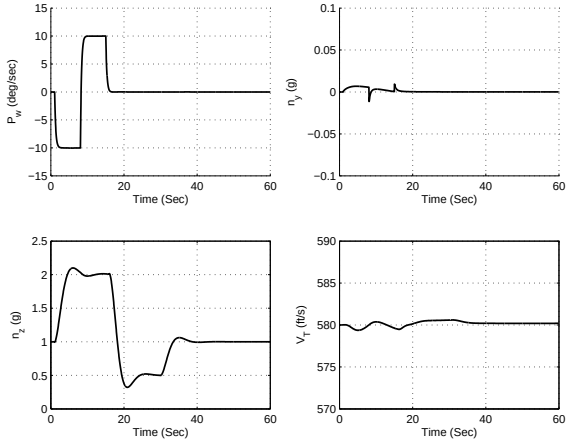

Fig. 18. Roll rate, Lateral acceleration, Normal acceleration and Total velocity in combined maneuver

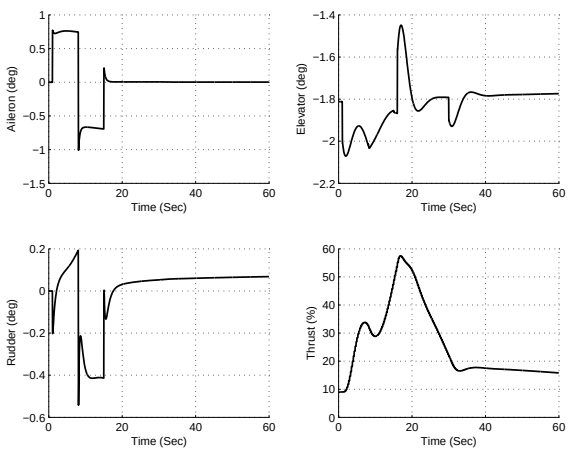

Fig. 19. Aileron, Elevator and Rudder deflections and Thrust level in combined maneuver

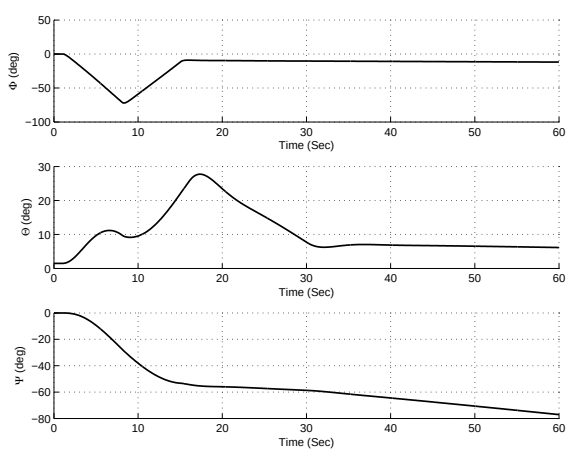

Fig. 20. Euler angles in combined maneuver

4.2.2. Neuro-Adaptive control design In this section, we present a set of representative results which shows that the adaptive control performs much better over the nominal control.

In the longitudinal mode, the pilot commands given (for which results are given here) are roll angle, normal and lateral acceleration and total velocity $[\phi,\ n_z,\ n_y,\ V_T]^T$. The necessary control histories and the associated tracking performance are given in Figures 22 and 23 respectively. Note that there are three plots in each of these figures, namely (i) the nominal plot (in which the nominal control is applied to the nominal plant), (ii) the actual plot (which represent the scenario in which the nominal control formula is applied to the actual plant with the actual state feedback) and (iii) the adaptive case, in which the adaptive control is applied to the actual plant. It is obvious from Figure 23 that the actual case leads to the control saturation in thrust (which opens the loop) and hence leads to failure in the tracking performance (see Figure 22). However the adaptive case does not lead to the control saturation and, as seen in Figure 22, the tracking performance is much better. In fact, the performance with adaptive control is so close to the nominal case that it feels as if there is no failure!

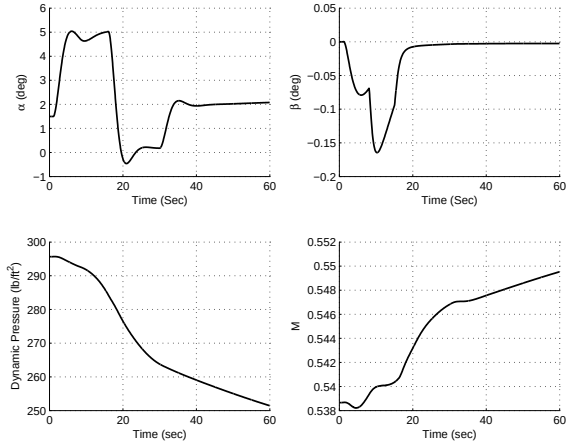

Fig. 21. Aerodynamic variables in combined maneuver

Similar results have been obtained in the lateral mode as well. In this case, the pilot commands assumed are roll rate, lateral acceleration, height and total velocity $[P,\ n_y,\ h,\ V_T]^T$. In our simulation studies we have noticed that the rudder deflection and the thrust go out of bounds for the actual case. However in the adaptive case these are well within the limits. In the tracking performance, the lateral acceleration and the total velocity goes away from the desired values for the actual case, whereas in the adaptive case they closely follow the desired values. Note that to contain the length we have not included the plots in this paper.

4.2.3. Robustness study for parameter inaccuracy Even though the results presented in Section is quite encouraging, to have a better idea of the robustness enhancement in performance, it is necessary to carry out further studies to infer about the robustness enhancement of the adaptive controller. To best of our knowledge, however, no systematic mathematical analysis tool is available for robustness analysis of nonlinear control designs. Hence, we have followed a probabilistic analysis approach from large number of simulation studies as an alternative (which can be interpreted as a Monte-Carlo simulation study).

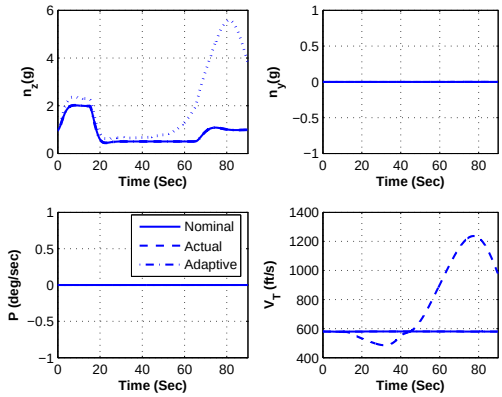

Fig. 22. Outputs in longitudinal maneuver

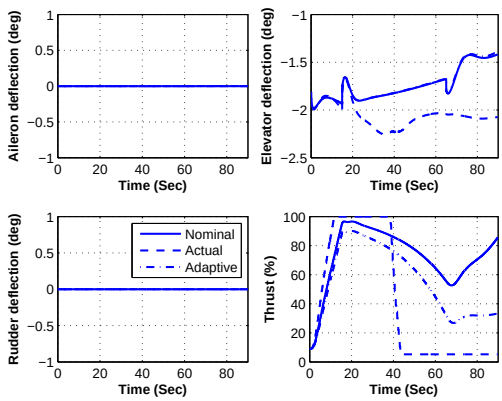

Fig. 23. Aileron, Elevator and Rudder deflections and Thrust level in longitudinal maneuver

In this study, first we perturbed the aerodynamic force and moment coefficients as well as the inertia parameters (i.e. mass and moment of inertia values) by various percentages of their nominal values. Then, we selected random numbers for each of the parameter values from within this bound using gaussian distribution, where mean value (μ) is taken as nominal value of the parameter and the standard deviation (σ) is taken as one-third of the maximum allowed perturbation in that parameter. Note that the controller was made ignorant of this perturbation.

In each simulation study, the aim was to declare it as either a 'success' or a 'failure' and then compute a probability of success from a large number of simulations. We decided to put a set of criteria for declaring a case as success, provided the maximum overshoot and steady state errors of the performance outputs are within the following limits: (i) n_z is within 20% of its commanded value (which is sufficiently large to expose the weakness of the nominal design), (ii) V_T is within 1% of its commanded value (1 % is taken since V_T itself is a high value), (iii)$-5\ deg < \Phi < 5\ deg$ and (iv) $-0.05g < n_y < 0.05g$. Note that absolute numerical bounds are necessary for Φ and n_y since their nominal values are zeros. A simulation run was considered as a success only if 'all' of the above conditions are satisfied. Similarly, in the lateral case with bank angle command option, we decided that the following bounds to be met for the maximum overshoot and steady state errors to declare a simulation run as a success: (i) Φ is within 10%, (ii) V_T is within 1%, (iii) h is within 1 % and (iv) $-0.05g < n_y < 0.05g$. Note that the percentage values are with respect to the corresponding commanded values. In the lateral case with roll rate command, however, the first condition is replaced with the condition that the overshoot and steady state error for P should remain within 10%. In the case of combined longitudinal and lateral maneuver case, we combined the criteria of longitudinal and lateral cases and decided that the following bounds should be met for the maximum overshoot and steady state errors to declare a simulation run as a success: (i) n_z is within 20%, (ii) P_w is within 10%, (iii) h is within 1% and (iv) $-0.05g < n_y < 0.05g$.

Next, we clubbed the aerodynamic coefficients into one group and the inertia parameters (mass and moment of inertias) into another. Then we put various combinations of their possible percentage errors at discrete values and for each such selected combination, ran 50 simulation case. From this exercise, we calculated the percentage of success and the results obtained are summarized in Table 4. Note that the two lateral cases have not been reported separately since the results obtained for them were found to be same for all perturbation cases.

From Table 4, the followings are evident:

- The nominal controller does not have sufficient robustness. Even for small 2% perturbations in aerodynamic parameters, there is robustness degradation. In fact, there is substantial amount of degradation for 5% and more perturbation of parameter values.
- With the application of adaptive control, for pure longitudinal and lateral modes the success was 100 % (there was no failure at all), even with 10% perturbation of parameter values. This obviously indicates substantial amount of robustness enhancement.
- The adaptive controller also leads to enhancement of robustness in combined lateral and longitudinal maneuvers. The success rate is not 100 % in this case (primarily because this is a punishing maneuver). However, with 10% perturbation of parameter values, the success rate observed was 84 %, which is quite high.

5. CONCLUSION

A new relatively straightforward approach based on dynamic inversion technique is presented in this paper for nonlinear flight control design of high performance aircrafts. This approach does not require the normal and lateral acceleration commands to be first trans-

Table 4. *Robustness in Various Modes*

Aerodynamic Coefficient Perturbation	1 %	1 %	2 %	2 %	5 %	5 %	10 %	10 %
Inertia Parameter Perturbation	5 %	10 %	5 %	10 %	5 %	10 %	5 %	10 %
Nominal Success	100 %	100 %	96 %	92 %	76 %	70 %	48 %	40 %
Adaptive Success(Longitudinal Mode)	100 %	100 %	100 %	100 %	100 %	100 %	100 %	100 %
Adaptive Success(Lateral Mode)	100 %	100 %	100 %	100 %	100 %	100 %	100 %	100 %
Adaptive Success(Combined Mode)	100 %	100 %	100 %	100 %	100 %	100 %	94 %	84 %

ferred to body rates before computing the required control inputs. This leads to substantial improvement of the tracking response, which is demonstrated from the six degree-of-freedom simulation studies of F-16 aircraft in longitudinal, lateral and combined longitudinal-lateral maneuvers. The new approach has two potential benefits, namely reduced oscillatory response (including elimination of non-minimum phase behavior) and reduced control magnitude. A model-following neuro-adaptive design has also been augmented the nominal design in order to assure robust performance in the presence of parameter inaccuracies in the model. The robustness study from a large number of simulations shows that the adaptive design enhances the robustness of the nominal design substantially.

Even though the results are quite promising, we wish to point out that an important possible direction of future research would be to test it in the presence of external noise (like wind guest, for example), sensor noise etc. To address this issue explicitly, a state estimator (say an extended Kalman filter) will be necessary in the loop. This may also open up the issue of 'data fusion' for better usage of the data from multiple sensors. Another possible direction of future research would be to do a careful rigorous comparison study of the adaptive control design proposed in this paper with one/more of the existing neuro-adaptive design ideas.

Acknowledgement

This research was supported by Defense Research and Development Organisation (DRDO)-India, under the contract CSSP/DRDO582 and CSSP/DRDO585.

REFERENCES

Bodson, M. (2002). A reconfigurable nonlinear autopilot. *AIAA Guidance, Navigation, and Control Conference and Exhibit, Monterey*, California, Aug. 5-8, 2002, AIAA-2002-4549.

Cloutier, J. R. (1997). State-Dependent Riccati Equation Techniques: An Overview. *Proceedings of the American Control Conference*, Jnue, 1997, Albuquerque, New Mexico, USA.

Enns, D., Bugajski, D., Hendrick, R., & Stein G. (1994). Dynamic Inversion: An Evolving Methodology for Flight Control Design. *International Journal of Control*, Vol.59, No.1, 71-91.

Gupta, S. K. (1995). Numerical Methods for Engineers. *Wiley Eastern Limited*.

Kaneshige, J., Bull, J., & Totah, J. J. (2000). Generic Neural Flight Control and Autopilot System. *AIAA Guidance, Navigation, and Control Conference and Exhibit*, Aug. 14 - 17, 2000, Denver, CO (A00-37116).

Keviczky, T., & Balas, G. J. (2006). Receding Horizon Control of an F-16 Aircraft: A Comparative Study. *Control Engineering Practice*, Vol.14 , 10231033.

Khalil, H. K. (2002). Nonlinear Systems. *Prentice Hall*, 3rd Edition.

Kim, B., & Calise, A. J. (1997). Nonlinear Flight Control Using Neural Networks. *Journal of Guidance, Control and Dynamics*, Vol.20, No.1, 26-33.

Lee, L. H., & Spillman, M. (1997). Robust, Reduced-Order, Linear Parameter-Varying Flight Control for an F-16. *Proc. of the 1997 AIAA Guidance, Navigation, and Control Conference*, AIAA Paper 97-3637.

Lin, C. F., Yu, T. J., Ge, J. H., Yeh, H. H., & Banda, S. S. (1997). Nonlinear H_∞ Flight Control System Design for Aircraft. *AIAA Guidance, Navigation, and Control Conference and Exhibit*, AIAA 97-3697.

Menon, P .K .A. (1993). Nonlinear Command Augmentation System for a High Performance Aircraft. *Proceedings of the AIAA Conference on Guidance, Navigation and Control*.

Morelli, E. A. (1998). Global Nonlinear Parametric Modeling with Application to F-16 Aerodynamics. *Proceedings American Control Conference*, Philadelphia, 997-1001.

Muir, E. (1998). The GARTEUR High Incidence Research Model (HIRM) benchmark problem. *AIAA Guidance, Navigation, and Control Conference and Exhibit*, Portland, Aug. 10 - 12, 1998, Collection of Technical Papers. Vol. 2 (A98-37001 10-63).

Nguyen, L. T., Ogburn, M. E., Gilbert, W. P., Kibler, K. S., Brown, P. w., & Deal, P. L. (1979). Simulator Study of Stall/Post-Stall Characteristics of a Fighter Airplane with Relaxed Longitudinal Static Stability*Technical Report*, Dec., 1979, NASA, 1538.

Ngo, A. D., Reigelsperger, W. C., & Banda, S. S. (1996). Multivariable control law design for a tailless airplane. *AIAA, Guidance, Navigation and Control Conference*, July 29-31, 1996, San Diego, CA, AIAA 96 3866.

Pachter, M. (1996). Velocity vector roll control. *AIAA, Guidance, Navigation and Control Conference*, July 29-31, 1996, San Diego, CA.

Padhi, R., Unnikrishnan, N., Balakrishnan, S. N. (2007). Model Following Neuro-Adaptive Control Design for Non-square, Non-affine Nonlinear Sy-

atem. *IET Control Theory and Applications* , Vol. 1, Issue 6, Nov. 2007, pp. 1650-1661.

Roskam, J. (1995). Airplane Flight Dynamics and Automatic Controls. *Darcorporation* , Part-1.

Russell, R. S. (2003). Nonlinear F-16 Simulation Using Simulink and Matlab. *Technical Report*, Version 1.0, University of Minnesota.

Schumacher, C. J., Cottrill, G. C. & Hsi-Han Yeh (1999). Robust, Reduced-Order, Linear Parameter-Varying Flight Control for an F-16. *AIAA Guidance, Navigation, and Control Conference and Exhibit*, Portland, Aug. 9 - 11, 1999, Collection of Technical Papers. Vol. 1 (A99-36576 09-63).

Shin, Y. J., Balas, G. J & Kaya, A. M. (2001). Blending Approach of Linear Parameter Varying Control Synthesis for F-16 Aircraft. *AIAA Guidance,Navigation and Control Conference and Exhibit*, 6-9 August, Montreal, Canada.

Soloway, D., & Haley, P. (2001). Aircraft Reconfiguration Using Neural Generalized Predictive Control. *Proceedings of The American Control Conference*, 2924-2929.

Wang, Q., & Stengel, R. F. (2005). Robust nonlinear flight control of a high-performance aircraft. *IEEE Transactions on Control Systems Technology* , Vol. 13, No. 1, 15 - 26.

Willis, P. A. (1999). Decentralised Adaptive Neuro-Fuzzy Longitudinal Control of High Performance Aircraft. *AIAA Guidance, Navigation, and Control Conference and Exhibit*, Portland, OR, Aug. 9-11, 1999, Collection of Technical Papers, Vol. 2 (A99-36576 09-63).

Won, T. H., Song, D. S., Nam, S. K., & Lee, M. H. (2004). A Design for Fuzzy Control for High Performance Aircraft. *Industrial Electronics, 1999. ISIE '99. Proceedings of the IEEE International Symposium*, 12 - 16 July, 1999, Bled, Slovenia.

Ying, H., Mirmirani, M., Ioannou, P., & Colgren. R. (2004). Adaptive Linear Quadratic Design with Application to F-16 Fighter Aircraft. *AIAA Guidance, Navigation, and Control Conference and Exhibit*, Aug. 16 - 19, 2004, Providence, Rhode Island.